Surface acoustic wave ammonia sensor based on SiO_2-SnO_2 composite film operated at room temperature

G D Long[a], Y J Guo[a,*], Y L Tang[b], J L Wang[a], Q B Tang[a], X F Xu[a], X T Zu[c], J Y Ma[d], B Du[d], H. Torun[e], Y Q Fu[e,*]

[a] School of Physics, University of Electronic Science and Technology of China, Chengdu, 610054, P. R. China

[b] School of Physical Science and Technology, Southwest Jiaotong University, Chengdu, 610031, P. R. China

[c] Institute of Fundamental and Frontier Sciences, University of Electronic Science and Technology of China, Chengdu, 610054, P. R. China

[d] Sichuan Institute of Piezoelectric and Acousto-Optic Technology, Chongqing, 400060, P. R. China

[e] Faculty of Engineering & Environment, University of Northumbria, Newcastle upon Tyne, NE1 8ST, UK

*Corresponding authors and E-mail addresses:

Prof. Yuanjun Guo (guoyuanjun@uestc.edu.cn);

Prof. Richard Yongqing Fu (richard.fu@northumbria.ac.uk).

Abstract

Sensitive thin film layers of SnO_2, SiO_2 and SiO_2-SnO_2 were deposited on a SAW resonator using sol-gel method and spin coating techniques. Their ammonia-sensing performance operated at room temperature was characterized and their sensing mechanisms were comprehensively studied. When exposed to ammonia, the sensors made of SnO_2 and SiO_2-SnO_2 films exhibit positive frequency shifts, whereas the SiO_2 film sensors exhibit a negative frequency shift. The positive frequency shift is related to the dehydration and condensation of hydroxyl groups, which make the films stiffer and lighter. The negative frequency shift is mainly caused by the increase of mass loading due to the adsorption of ammonia. The gas sensor based on SiO_2-SnO_2 film shows a positive frequency shift of 631 Hz when it is exposed to ammonia with a low concentration of 3 ppm, and it also shows good repeatability and stability, as well as a good selectivity to ammonia compared with gases of C_6H_{14}, C_2H_5OH, C_3H_6O, CO, H_2, NO_2, and CH_4.

Keywords**:** Surface acoustic wave (SAW); Ammonia sensor; SnO_2; SiO_2; Composite film.

1. Introduction

Ammonia (NH_3) is a colorless and toxic gas with a strong irritating odor, widely used in pharmaceutical, chemical industries and national security [1-6]. At high concentration levels, it is harmful to skin, eyes, throat and lungs, resulting in permanent blindness and chronic lung diseases. Considering its widespread usages and health hazards, it is critical to develop ammonia sensors with good selectivity, high response, high resolution and long-term stability. So far, various types of ammonia sensors have been developed including metal oxide semiconductor sensors, electrochemical sensors and surface acoustic wave (SAW) sensors, etc. [7-16].

Due to its advantages of having high sensitivity, fast response, high resolution and being immune to electromagnetic interferences, SAW devices have been widely used for gas sensing [12, 17, 18, 19]. The key principle of a SAW gas sensor is based on the interaction of the targeted gas molecules with a sensitive film, which results in changes in resonant frequency of the waves travelling on the surface of the sensor [20-22]. The changes in the effective mass of the film (mass loading), modulus of elasticity/density/viscosity (elastic loading) or the conductivity (electric loading) can change the resonant frequency of the SAW devices [22-25]. Up to now, many materials have been used to detect ammonia gas, such as indium oxide (In_2O_3), titanium oxide (TiO_2), cerium oxide (CeO_2), carbon nanotubes and graphene [26–33]. Tin oxide (SnO_2) is one of the most widely used sensitive materials because of its sensitivity to various toxic and organic gases [34-36]. However, SnO_2-based gas sensors have some obvious problems such as high optimum working temperature, poor selectivity and poor

stability [37-39]. Synthesis of SnO_2-based composite with other types of oxides is considered as one of the effective ways to alleviate the shortcomings of SnO_2 based gas sensors [40].

The surface of SiO_2, SnO_2 and composite SiO_2-SnO_2 films prepared with a sol-gel technology at the atmospheric pressure and room temperature is rich in hydroxyl groups [41,42], even after post-annealing [42,43]. Hydroxyl has a strong water absorption capability as it forms hydrogen bonds with water molecules. This property is advantageous for ammonia sensing attributed to the high water solubility of ammonia as demonstrated with various SiO_2-based sensors [44-46]. SiO_2-SnO_2 composite materials can take the advantages of the desirable properties of SiO_2. Because of the porous surface of SiO_2 prepared using the sol-gel method, the specific surface area of SiO_2-SnO_2 will become larger than that of pure SnO_2 layer, thus enhancing its capability of adsorbing ammonia [47]. In addition, it is reported that hydroxyl groups on the SiO_2 become dehydrated and polymerized under the catalysis of ammonia [48-50], which would make the film stiffer and a little lighter (after hydroxyl condensation, the active sites of adsorbing water molecules will be reduced, and the corresponding water molecules on the surface of the film will be reduced). The structural change results in significant changes in the behavior of travelling waves on the surface of SAW sensors. Consequently, SiO_2-SnO_2 can be used as a good NH_3 sensing material.

In this paper, NH_3 gas sensors based on SnO_2-SiO_2 composite films were fabricated. Their ammonia-sensing performance was characterized at room temperature and their sensing mechanisms were comprehensively investigated . The experimental results

show that the presence of SiO_2 enhances the sensitivity and the selectivity of the sensor to ammonia at room temperature. In addition, effect of humidity on sensing behavior was also investigated.

2. Experimental details

2.1 Materials

Tin chloride dihydrate, tetraethoxysilanc (TEOS), ammonia (analytic pure liquid, 25 wt%) and ethanol, all in an analytical purity, were purchased from Tianjin Regent Chemicals limited company, China. Commercially standard gases of NH_3 (2 vol%), CH_4 (2 vol%), H_2 (2 vol%), CO (2 vol%) and NO_2 (2 vol%) in dry nitrogen were purchased from the National Institute of Measurement and Testing Technology, China. The two-port SAW resonator device was fabricated using a standard photolithography process. 200 nm-thick aluminum was deposited on an ST-cut（42°75′） quartz substrate (12 mm × 3 mm × 0.5 mm). A lift-off process was used to prepare aluminum interdigital transducers (IDTs, two sets of 30 pairs) with a periodicity of 16 μm and reflective gratings (100 pairs), as shown in Fig.1. The propagation direction of the generated SH-SAW is perpendicular to the crystallographic x-axis (90°-rotated). The designed resonant frequency of the SAW device is 200 MHz.

2.2 Sensor fabrication

The Stöber method was used to prepare SiO_2 sol [51]. The TEOS (high purity), deionized water, ethanol (analytical purity) and ammonia (analytical purity, 25 wt%) were added into a Bunsen flask using a magnetic stirrer for 30 min to obtain a silica sol with a molar ratio of 37:3.25:1:0.17. SnO_2 sol was prepared according to the following

steps. Firstly, 5.64125 g of tin chloride dihydrate was added to 50 ml ethanol followed by 2 ml glycerol. The mixed solution was stirred for 2 hours at 70° C. After stabilizing the solution for one day, a tin dioxide sol can be obtained. SiO_2-SnO_2, SiO_2-$2SnO_2$ and $2SiO_2$-SnO_2 sols were prepared by mixing SiO_2 and SnO_2 sols at mole ratios of 1:1, 1:2 and 2:1 using a magnetic stirrer for 1 hour, respectively.

SiO_2, SnO_2 and SiO_2-SnO_2 composite sols were spin coated onto SAW resonator fort two cycles with a speed of 5000 r/min for 30 seconds in each cycle. The device was then annealed at 400℃ for 2 hours at atmospheric conditions. A schematic diagram of the SAW sensor is shown in Fig. 2 (a). The SAW sensor is based on an oscillator which consists of a sensing film coated SAW resonator with its corresponding amplifying and phase-shift circuits. The gas sensing set-up using the SAW sensor is shown in Fig. 2 (b).

2.3 Characterizations

An X-ray diffractometer（XRD, Bruker D2 PHASER) and a field-emission scanning electron microscope (SEM, FEI Inspect F) were used to characterize the crystallinity and morphology of the prepared films. An Fourier transform infrared (FTIR) Spectrometer (Nicolet 6700) was used to obtain the infrared absorption spectra of the prepared films. A four point probe (Sx 1944) was used to measure the sheet conductivity of the films coated on a K9 glass. Digital power meter (Keithley 2200-60-2) was used to measure changes in the conductance of sensors when exposed to ammonia. A vector network analyzer (HP-8714C) was used to measure the resonant frequency and transmission signals of S_{21} parameter and the results are shown in Fig. 3. From the

figure, we can see that the center frequency of S_{21} is 200.03 MHz, and the insertion loss is -8.486 dB.

The SAW gas sensing experiments were performed at the room temperature of 25℃. During the measurement, the relative humidity (RH) of the environment was set to be 40% using a humidifier. The sensor was installed in a large plastic box with a volume of 20 liters. A precisely controlled syringe was used to inject ammonia into the testing box. The concentration of ammonia in the test chamber was accurately controlled by a dynamic volumetric method. For example, 10 milliliter of standard ammonia is mixed with 20 liters of air in an 40% relative humidity environment to obtain 10 ppm of ammonia. Different concentrations of ammonia were obtained by controlling the volume of injected ammonia into the chamber.

The resonant frequency of the sensor was recorded using a frequency counter (Agilent 53132A) as shown in Fig. 2. For the recovery testing of the SAW sensor, when the sensor's response became stable with the ammonia gas, the chamber was opened, and thus the sensor was exposed to the ambient atmosphere to test its recovery performance, and the frequency of the SAW devices was monitored. The response of the sensor is defined as $\Delta f = f_s - f_0$ where f_s and f_0 are measured resonant frequencies in the ammonia environment and in the air, respectively. The time for the sensor to reach 90% of the total frequency shift is defined as the response time, and the time for the sensor to recover to 10% of the total frequency shift is defined as the recovery time.

3. Results and discussion

3.1 Film characterization

Fig. 4 shows XRD results of SiO_2, SnO_2, and SiO_2-SnO_2 films. The peak of the SiO_2 is quite broad, showing a typical feature of the amorphous SiO_2 (JCPDS file 29-0085). It is obvious that peaks can be observed at 29, 35, 41 and 51 degrees., corresponding to (1 1 0), (1 0 1), (2 0 0) and (2 1 1) planes of SnO_2 (JCPDS file 41-1445, respectively. This is in a good agreement to the corresponding values reported for rutile structure of SnO_2 [52]. The XRD pattern of the SiO_2-SnO_2 composite film consists of those of the SnO_2 and SiO_2 thin films. Therefore, it is believed that there are amorphous SiO_2 and rutile SnO_2 in the prepared SiO_2-SnO_2 films.

The typical infrared spectra of SiO_2, SnO_2, and SiO_2-SnO_2 films are shown in Fig. 5. Within the range of high wave numbers, there are broad bands in three spectra between 2800 and 3600 cm^{-1}, which are linked with the hydroxyl group of the telescopic vibration mode [43]. The bands at 1630 cm^{-1} are related to water deformation [43]. In the SiO_2 spectrum (Fig. 5(a)), the peaks at 468, 794, and 1084 cm^{-1} correspond to its transverse optical (TO) modes, and TO_1, TO_2 and TO_3 at 468 cm^{-1}, 794 cm^{-1} and 1084 cm^{-1}, respectively [43]. In the spectrum of SnO_2 (Fig. 5(b)), there is a wide and strong band in the 400~800 cm^{-1} associated to Sn-O-Sn stretching vibrations which is belonged to Sn–OH groups. Other peaks from 1300 to 1500 cm^{-1} can be allocated to residual carbon [42]. The spectra of composite SiO_2-SnO_2 in Fig. 5(c) confirm that SiO_2 and SnO_2 coexist in the tested samples.

From the FTIR results, it can be seen that hydroxyl groups exist in all three films. Therefore, all samples can easily adsorb water molecules in the environment. When

these samples are exposed to ammonia gas, hydroxyl groups will adsorb water molecules, which will then adsorb ammonia gas (ammonia is highly soluble in water) and make the film much heavier. At the same time, the absorption of ammonia gas may also cause hydroxyl condensation and polymerization, thus making the film stiffer and lighter. Therefore, all three films can be used as ammonia sensitive films for SAW sensors.

The SEM images of the surface morphologies of SiO_2, SnO_2 and SiO_2-SnO_2 composite films are shown in Fig. 6. It can be seen clearly that SiO_2 thin films are composed of many SiO_2 particles with a diameter of about 35 nm with many voids/cracks in the film. Pure SnO_2 thin films exhibit a finer and denser structure with an average particle size of 12 nm without obvious defects. The maximum particle size of SiO_2-SnO_2 composite films is 62 nm with significant area coverage of defects observed. High porosity and roughness of the surface can promote diffusion of gas molecules into the film, thus enhancing the performance.

3.2 Gas sensing properties

Fig. 7 shows the responses of various films to ammonia with a concentration of 10 ppm. Results show that frequency shift of SiO_2 film is negative, whereas those of other films are positive, and the reason will be discussed later. As far as the magnitude of frequency shifts among the three mixed films are concerned, only the response of $2SiO_2$-SnO_2 film is smaller than that of pure SnO_2 film; and SiO_2-SnO_2 composite film has the highest response among the composite films, with a frequency shift of 2.16 kHz.

Fig. 8(a) shows the dynamic responses of the sensor based on the pure SnO_2 film to

a sequence of NH_3 with concentrations of 10 ppm, 20 ppm, 40 ppm, 60 ppm, 80 ppm, and their corresponding frequency shifts are 0.66 kHz, 0.853 kHz, 1.156 kHz, 1.249 kHz and 1.431 kHz, respectively. Fig. 8(b) shows the dynamic responses of the sensors with SiO_2-SnO_2 composite film to a sequence of NH_3 gas concentration of 3 ppm, 5 ppm, 10 ppm, 20 ppm, 40 ppm, 60 ppm, 80 ppm at room temperature. The measured frequency shifts are 0.643 kHz, 1.597 kHz, 2.163 kHz, 2.584 kHz, 3.398 kHz, 4.108 kHz and 4.792 kHz, respectively. It can be clearly seen that the responses of two sensors are increased with the increase of ammonia concentration. However, the SiO_2-SnO_2 composite film can detect lower concentrations (down to 3 ppm) of ammonia than the pure SnO_2 film. The frequency shifts of the SiO_2-SnO_2 film are larger and their responses are more significant. The responses and recovery time of SiO_2-SnO_2 composite film sensor under different ammonia concentrations are shown in Fig. 9. The response time has some fluctuations, but the data are all less than 300 seconds, and the recovery time is slightly longer, ranging from 200 to 650 seconds.

The selectivity of the SiO_2-SnO_2 composite film sensor and pure SnO_2 sensor was characterized using eight different types of gases (C_6H_{14}, C_2H_5OH, C_3H_6O, CO, H_2, NO_2 and CH_4 and NH_3). As shown in Fig. 10 (a), although the responses of pure SnO_2 sensor to C_6H_{14}, C_3H_6O, CO, H_2 and CH_4 are reasonably low, the differences in the total frequency shifts between C_2H_5OH, NO_2 and NH_3 are relatively small, indicating a poor selectivity. As shown in Fig. 10 (b), the SiO_2-SnO_2 composite film-based SAW sensor is significantly better in terms of selectivity to NH_3 and shows low responses to all the other seven types of gasses. As there are many hydroxyl groups on the surface of the

composite film, they will act as the active sites to adsorb the water molecules in the air. Meanwhile, the solubility of ammonia in the water is very large, which can reach 700:1. This could be the reason why the SiO_2-SnO_2 composite based SAW sensor has a good response toward ammonia gas.

Four sensing cycles were performed at room temperature with the sensor exposed to NH_3 with a concentration of 5 ppm in order to evaluate the repeatability of SiO_2-SnO_2 composite film sensor. As shown in Fig. 11, the responses of SiO_2-SnO_2 composite film sensor for four different cycles are 1.58 KHz, 1.55 KHz, 1.61 KHz and 1.53 KHz. These results indicate a good short-term stability, with a frequency fluctuation less than 5%.

Six separate experiments were carried out in 42 days using the SiO_2-SnO_2 composite film sensor to investigate its long-term stability. In each experiment, SiO_2-SnO_2 composite film sensors were continuously exposed to NH_3 with concentrations of 3 ppm, 20 ppm and 60 ppm. The experiments were conducted every 7 days, and the results of six tests are shown in Fig. 12. Obviously, the sensor has a stable response to different concentrations of NH_3 within 42 days.

3.3 Sensing mechanism

The resonant frequencies of SAW sensors are affected by three main factors: the sheet conductivity (electric loading), the Young's modulus (elastic loading) and the mass loading on the film (mass loading) [53].

Electroacoustic effect means the electrical properties (especially conductivity and dielectric properties) of the sensing films will be changed due to the adsorption of target gas molecules [53]. When the target gas molecules are absorbed and diffused into the

sensing film, if the conductivity of the film increases, the central frequency of the SAW device will decrease, thus resulting in a negative frequency shift, and vice versa. The relationship between frequency shift and charge load is as follows [53, 54]:

$$\Delta f = -f_0 \times \frac{K^2}{2} \times \left(\frac{1}{1+\left(\frac{V_0 C_s}{\sigma_s}\right)^2} \right) \quad (1)$$

where, f_0 (200 MHz) is the unperturbed oscillation frequency of the sensor, V_0 (for substrate of ST-cut quartz, 3158 m/s) is the unperturbed surface acoustic wave velocity on the SAW resonator, K^2 (0.0011) is the electromechanical coupling coefficient, C_s (0.5 pF/cm) is the capacitance per unit length of the SAW resonator fabricated on a ST-cut quartz substrate. σ_s is the sheet conductivity of the sensing film. We can define a normalized response as $R = R_{air}\text{-}R_{gas}/R_{gas}$, where R_{air} and R_{gas} are the film resistances in ambient air and exposure in ammonia, respectively. As shown in Fig. 13, the increase of R value of these three sensors are less than 3.4 times to 10 ppm NH_3. The relationship between normalized frequency shifts with different acoustoelectric parameters ($\frac{\sigma_s}{V_0 C_s}$) are show in Fig. 14. Figure 15 shows a schematic illustration of the four-probe test. Four probes arranged in a line are pressed vertically on the surface of the sample to be tested, and a current I (mA) is passed between the probes 1 and 4. A voltage V (mV) is applied between the probes 2 and 3, and the measured data of conductivity are calculated as listed in Table 1. Based on the results, σ_s values of all the sensing films are increased due to exposure to ammonia, which are lower than 10^{-8} S square. According to formula (1), the values of Δf for the SiO_2, SnO_2 and SiO_2-SnO_2 composite film sensors when exposed to ammonia gas of 10 ppm are calculated as -1.82×10^{-2} Hz、-2.39 Hz and -2.72 Hz, respectively. Therefore, it can be seen that

electric loading is not the major factor affecting Δf in this study.

The influence of mass loading on thin film on sensor is expressed by the following formula [55],

$$\Delta f = (k_1 + k_2) \times f_0^2 \times \Delta \rho_s \quad (2)$$

where $k_1(-8.7 \times 10^{-8} m^2 s k g^{-1})$ and $k_2(-3.9 \times 10^{-8} m^2 s k g^{-1})$ are substrate material constants of ST cut quartz. $\Delta \rho_s$ is the change of density for the sensing film of SAW sensor exposed to ammonia. It should be noted that k_1 and k_2 have both negative signs, therefore a positive change $\Delta \rho_s$ will lead to a negative value of Δf.

Another influencing factor is the elastic loading. When the elastic modulus changes, the propagation of surface acoustic wave will be disturbed, and the center frequency will be changed. When the sensitive films adsorb gas molecules, the viscoelasticity of the films will be changed, and the generated stress will be imposed onto the quartz substrate. If the adsorbed gas molecules cause densification of the film, the central frequency of the sensor will be increased. The relationship between frequency shift and elasticity load is given in the following formula [55],

$$\Delta f = p \Delta E \quad (3)$$

where p is a positive constant. ΔE is the change of elastic modulus of sensitive film exposed to ammonia. When the rigidity of film increases, ΔE becomes positive, and the frequency shift Δf of sensor will be positive.

Two possible sensing mechanisms for sensors are defined as process 1 and process 2, respectively, as shown in Fig.16. Since there are hydrophilic hydroxyl groups on the surfaces of SnO_2, SiO_2 and SiO_2-SnO_2 composite films, therefore, it is easy to capture

water molecules in the air, which are then adhered to the film surface, as shown in Fig.16 (a). The absorbed water can promote adsorption of ammonia because of its high solubility in water, adding the mass of the film as shown in Fig. 16 (b). According to the formula 2, a downshift in the resonant frequency will be observed. The hydroxyls on the films are catalyzed by absorbed NH_3 to become condensation (Fig. 16 (c)), and thus the film becomes stiffer and lighter. Therefore, the Δf will be increased according to formula (2) (3) as a result of process (2).

In order to understand the reason why the response of SiO_2-SnO_2 composite film is significantly higher than that of SnO_2 film, RH values were changed from 5% to 40% and from 40% to 70% to studied the responses of the sensor. The obtained results are show in Figs. 17(a) and 17(b), respectively, with the details data summarized in Table 2. The mass loading effect is increased as the hydroxyl groups adsorb water, resulting in a negative frequency shift. It can be seen from Table 2 that compared with SnO_2 film sensor, both the SiO_2 film sensors and SiO_2-SnO_2 film sensors have shown more negative frequency shifts under the same humidity change, so they are more sensitive to the change of RH.

The amount of ammonia adsorbed on SiO_2-SnO_2 films is much higher than that adsorbed on pure SnO_2 films, which makes the SiO_2-SnO_2 film sensors more sensitive than SnO_2 films. To verify the above results, we tested the response of SiO_2, SnO_2 and SiO_2-SnO_2 thin film sensors to 10 ppm NH_3 at different relative humidity values as show in Figs. 18 (a) to 19(c). Obviously, with the increase of relative humidity, the responses of all sensors are increased, which supports the aforementioned conclusion.

The response and recovery curves of SiO_2 thin film, SnO_2 thin film and SiO_2-SnO_2 film are compared in Fig. 19. During the response process, for SnO_2 and SiO_2-SnO_2 thin films, it is obvious that the frequency shifts are positive and the sensing mechanism can be considered as process (2). Whereas for SiO_2 thin films, the frequency shift is negative, which is attributed to the process (1) as shown in Fig. 16. Contrary to the response process, processes (1) and (2) shown in Fig. 16 during the recovery process cause positive and negative frequency shifts, respectively. In the recovery process, the recovery time of SnO_2 and SiO_2-SnO_2 films is 232 seconds and 239 seconds, respectively, while that of SiO_2 films is 91 seconds. In process (1), the adsorption of ammonia in the thin film is mainly caused by physical adsorption, so the time required for the desorption process of physical adsorption is relatively short. In process (2), ammonia-catalyzed membrane leads to hydroxyl dehydration polymerization, which is more complex than physical adsorption, therefore the response time of the adsorption is longer. Therefore, we can conclude that the sensing mechanism of SiO_2 thin film is mainly the process (1) and the sensing mechanisms of SnO_2 thin films and SiO_2-SnO_2 thin films are mainly the process (2) as shown in Fig. 16.

4. Conclusion

In summary, the ST-cut quartz SAW ammonia sensor was fabricated based on SiO_2-SnO_2 composite film. Results show that all the sensors respond well to ammonia measured at room temperature. When exposed to ammonia, sensors made of SnO_2 and SiO_2-SnO_2 films exhibit positive frequency shifts, while those of SiO_2 films exhibit negative frequency shifts. The characterization experiments reveal that the negative

frequency shift of SiO_2 thin film sensor is mainly due to the adsorption of water molecules for the hydroxyl groups on the thin film, which results in an increase of mass loading due to the adsorption of ammonia. The positive frequency shifts of both the SnO_2 and SiO_2-SnO_2 thin film sensors are related to hydroxyl catalytic condensation. When exposed to ammonia, dehydration and condensation of hydroxyl groups make the film harder and lighter. Through the analysis of the responses of the sensors under various conditions in humidity, we find that the SiO_2-SnO_2 film has the highest sensitivity to ammonia, along with its excellent repeatability, stability and selectivity.

Acknowledgments

The authors acknowledge the support by the Fundamental Research Funds for the Central Universities (A03018023801119), Funding supports from UK Engineering Physics and Science Research Council (EPSRC EP/P018998/1), Newton Mobility Grant (IE161019) through Royal Society and NFSC, and Royal academy of Engineering UK-Research Exchange with China and India are also acknowledged.

References

[1] X. Li, X. Li, Z. Li, J. Wang, J. Zhang, WS_2 nanoflakes based selective ammonia sensors at room temperature, Sens. Actuators B Chem. 240 (2017) 273-277.

[2] C.F. Eno, G.B. William, M.G. Joseph, The effect of anhydrous ammonia on nematodes fungi, bacteria, and nitrification in some Florida soils, Soil Sci. Soc. Am. J. 19 (1955) 55-58.

[3] E. Stokstad, Ammonia pollution from farming may exact hefty health costs, Science

343 (2014) 238-338.

[4] J.M. Bremner, G.A. Breitenbeck, A.M. Blackmer, Effect of anhydrous ammonia fertilization on emission of nitrous oxide from soils, J. Environ. Qual. 10 (1981) 77-80.

[5] R.A. Michaels, Emergency planning and the acute toxic potency of inhaled ammonia, Eenviron Health Persp. 107 (1999) 617.

[6] W. Ament, J.R. Huizenga, E. Kort, T.W. Van Der Mark, R.G. Grevink, G.J. Verkerke, Respiratory ammonia output and blood ammonia concentration during incremental exercise, Int. J. Sports Med. 20 (1999) 71-77.

[7] D.Z. Zhang, Z.M. Yang, P. Li, M.S. Pang, Q.Z. Xue, Flexible self-powered high-performance ammonia sensor based on Au-decorated $MoSe_2$ nanoflowers driven by single layer MoS_2-flake piezoelectric nanogenerator, Nano Energy. 65 (2019) 103974.

[8] D.Z. Zhang, C.X. Jiang, P. Li, Y. Sun, Layer-by-Layer Self-assembly of Co_3O_4 Nanorod-Decorated MoS_2 Nanosheet-Based Nanocomposite toward High-Performance Ammonia Detection, ACS Appl. Mater. Interfaces 9 (2017) 6462-6471.

[9] D.Z. Zhang, Z.L. Wu, X.Q. Zong, Y. Zhang, Fabrication of polypyrrole/Zn_2SnO_4 nanofilm for ultra-highly sensitive ammonia sensing application, Sensor. Actuat. B-Chem. 274 (2018) 575-586.

[10] D.Z. Zhang, Z.L. Wu, P. Li, X.Q. Zong, G.K. Dong, Y. Zhang, Facile fabrication of polyaniline/multi-walled carbon nanotubes/molybdenum disulfide ternary nanocomposite and its high-performance ammonia-sensing at room temperature, Sensor. Actuat. B-Chem. 258 (2018) 895-905.

[11] D.Z. Zhang, J.J. Liu, C.X. Jiang, A.M. Liu, B.K. Xia, Quantitative detection of formaldehyde and ammonia gas via metal oxide-modified graphene-based sensor array combining with neural network model, Sensor. Actuat. B-Chem. 240 (2017) 55-65.

[12] S.Y. Wang, J.Y. Ma, Z.J. Li, H.Q. Su, N.R. Alkurd, W.L. Zhou, L. Wang, B. Du, Y.Tang, D. Ao, S. Zhang, Q. Yu, X. Zu, Surface acoustic wave ammonia sensor based on ZnO/SiO_2 composite film, J. Hazard. Mater. 285 (2015) 368-374.

[13] B. Timmer, W. Olthuis, A. Van Den Berg, Ammonia sensors and their applications-a review, Sensor. Actuat. B-Chem. 107 (2005) 666-677.

[14] D. Sil, J. Hines, U. Udeoyo, E. Borguet, Palladium nanoparticle-based surface

acoustic wave hydrogen sensor, ACS Appl. Mater. Interfaces 10 (2015) 5709-5714.

[15] Y.L. Tang, Z.J. Li, J.Y. Ma, H.Q. Su, Y.J. Guo, L. Wang, B. Du, J. Chen, W. Zhou, Q. Yu, X.T. Zu, Highly sensitive room-temperature surface acoustic wave (SAW) ammonia sensors based on Co_3O_4/SiO_2 composite films, J. Hazard. Mater. 280 (2014) 127-133.

[16] N. Fourati, M. Seydou, C. Zerrouki, A. Singh, S. Samanta, F. Maurel, D.K. Aswal, M. Chehimi, Ultrasensitive and selective detection of dopamine using cobalt-phthalocyanine nanopillar-based surface acoustic wave sensor, ACS Appl. Mater. Interfaces 24 (2014) 22378-22386.

[17] Y.L. Tang, Z.J. Li, X.T. Zu, J.Y. Ma, L. Wang, J. Yang, B. Du, Q.K. Yu, Room-temperature NH_3 gas sensors based on Ag-doped γ-Fe_2O_3/SiO_2 composite films with sub-ppm detection ability, Journal of Hazardous Materials 298 (2015) 154-161.

[18] J. Devkota, K.J. Kim, P.R. Ohodnicki, J.T. Culp, D.W. Greved, and J.W. Lekse, Zeolitic imidazolate framework-coated acoustic sensors for room temperature detection of carbon dioxide and methane，Nanoscale, 10 (2018) 8075

[19] R. Lucklum, C. Behling, P. Hauptmann, Role of mass accumulation and viscoelastic film properties for the response of acoustic-wave-based chemical sensors, Anal. Chem. 71 (1999) 2488-2496.

[20] A.J. Ricco, S.T. Martin, T.E. Zipperian, Surface acoustic wave gas sensor based on film conductivity changes, Sensor. Actuat. 8 (1985) 319-333.

[21] D.Y. Gallimore, P.J. Millard, M. Pereira da Cunha, Monitoring polymer properties using shear horizontal surface acoustic waves, ACS Appl. Mater. Interfaces 10 (2009) 2382-2389.

[22] Z. Y. Tang, J. Li, L. Ma, J. Wang, B. Yang, Q. Du, X. Zu Yu, Highly sensitive surface acoustic wave (SAW) humidity sensors based on sol-gel SiO_2 films: investigations on the sensing property and mechanism, Sensor. Actuat. B-Chem 215 (2015) 283-291

[23] R. Lucklum, C. Behling, P. Hauptmann, Role of mass accumulation and viscoelastic film properties for the response of acoustic-wave-based chemical sensors, Anal. Chem. 71 (1999) 2488–2496.

[24] A.J. Ricco, S.T. Martin, T.E. Zipperian, Surface acoustic wave gas sensor based on film conductivity changes, Sensor. Actuat. 8 (1985) 319–333.

[25] D.Y. Gallimore, P.J. Millard, M. Pereira da Cunha, Monitoring polymer properties using shear horizontal surface acoustic waves, ACS Appl. Mater. Interfaces 10 (2009) 2382–2389.

[26] L. Dai, Y.G. Liu, W. Meng, G.X. Yang, H.Z. Zhou, Z.X. He, Y.H. Li, L. Wang, Ammonia sensing characteristics of $La_{10}Si_5MgO_{26}$-based sensors using In_2O_3 sensing electrode with different morphologies and CuO reference electrode, Sens. Actuators B: Chem. 228 (2016) 716-724.

[27] W. Meng, L. Dai, W. Meng, H. Zhou, Y. Li, Z. He, L. Wang, Mixed-potential type NH3 sensor based on TiO_2 sensing electrode with a phase transformation effect, Sens. Actuators B Chem. 240 (2017) 962-970.

[28] J.Q. Wang, Z.J. Li, S Zhang, S.G. Yan, B.B. Cao , Z.G. Wang, Y.Q. Fu, Enhanced NH3 gas-sensing performance of silica modified CeO_2 nanostructure based sensors. Sensors and Actuators B 255 (2018) 862-870

[29] T. Zhang, M.B. Nix, B.-Y. Yoo, M.A. Deshusses, N.V. Myung, Electrochemically functionalized single-walled carbon nanotube gas sensor, Electroanalysis 18 (2006) 1153-1158.

[30] J.-W. Han, B. Kim, J. Li, M. Meyyappan, A carbon nanotube based ammonia sensor on cotton textile, Appl. Phys. Lett. 102 (2013) 193104.

[31] Y.L. Tang, D.Y. Ao. W. Li, X.T. Zu, S. Li, Y.Q. Fu, NH_3 sensing property and mechanisms of quartz surface acoustic wave sensors deposited with SiO_2, TiO_2, and SiO_2-TiO_2 composite films, Sens. Actuators B: Chem. 254 (2018) 1165-1173.

[32] N. Hu, Z. Yang, Y. Wang, L. Zhang, X. Huang, H. Wei, L. Wei, Y. Zhang, Ultrafast and sensitive room temperature NH_3 gas sensors based on chemically reduced graphene oxide, Nanotechnology 25 (2014) 025502.

[33] M. Gautam, A.H. Jayatissa, Graphene based field effect transistor for the detection of ammonia, J. Appl. Phys. 112 (2012) 064304.

[34] Barsan, N, Weimar, U, Understanding the fundamental principles of metal oxide based gas sensors; the example of CO sensing with SnO_2 sensors in the presence of

humidity，Journal of Physics Condensed Matter, 15 (2003) 20

[35] A. Katsuki， K. Fukui, H_2 selective gas sensor based on SnO_2，Sensors and Actuators B: Chemical, (1998) 30-37

[36] Q. Wan，T. H. Wang，Single-crystalline Sb-doped SnO_2 nanowires: synthesis and gas sensor application，Chemical Communications, 30 (2005) 3841-3

[37] Chen, W.; Zhou, Q.; Gao, T.; Su, X.; Wan, F. Pd-doped SnO_2-based sensor detecting characteristic fault hydrocarbon gases in transformer oil. J. Nanomater. 2013 (2013) 1-9.

[38] Kim, K.; Choi, K.; Jeong, H.; Kim, H.J.; Kim, H.P.; Lee, J. Highly sensitive and selective trimethylamine sensors using Ru-doped SnO_2 hollow spheres. Sens. Actuators B Chem., 166 (2012) 733-738.

[39] Wang, D.; Chu, X.; Gong, M. Gas-sensing properties of sensors based on single crystalline SnO_2 nanorods prepared by a simple molten-salt method. Sens. Actuators B Chem., 117 (2006) 183-187.

[40] Z.J. Li, H. Li, Z.L. Wu, J.T. Luo, H. Torun, P.A. Hu, C. Yang, M. Grundmann, X.T. Liu, Y.Q. Fu, Advances in designs and mechanisms of semiconducting metal oxide nanostructures for high-precision gas sensors operated at room temperature, Mater. Horiz, 6(2019)470.

[41] T.M. Parrill, Transmission infrared study of acid-catalyzed sol-gel silica coatings during room ambient drying, J. Mater. Res. 7 (1992) 2230-2239.

[42] Kuantama E, Han DW, Sung YM, Song JE, Han CH, Structure and thermal properties of transparent conductive nanoporous F:SnO_2 films, Thin Solid Films 517 (2009) 4211

[43] N. Primeau, C. Vautey, M. Langlet, The effect of thermal annealing on aerosol-gel deposited SiO_2 films: a FTIR deconvolution study, Thin Solid Films 310 (1997) 47-56.

[44] Sneh, S.M. George, Thermal stability of hydroxyl groups on a well-defined silica surface, J. Phys. Chem. 99 (1995) 4639-4647.

[45] N.H. de Leeuw, F.M. Higgins, S.C. Parker, Modeling the surface structure and stability of -quartz, J. Phys. Chem. B 103 (1999) 1270-1277.

[46] B.J. Meulendyk, M.C. Wheeler, M.P. da Cunha, Hydrogen fluoride gas detection

mechanism on quartz using SAW sensors, IEEE Sens. J. 11 (2011) 1768-1775.

[47] A. Martucci, N. Bassiri, M. Guglielmi, L. Armelao, S. Gross, J.C. Pivin, NiO-SiO_2 sol-gel nanocomposite films for optical gas sensor, J. Sol-gel Sci. Tech. 26 (2003) 993-996.

[48] F.P. Belleville, H.G. Floch, Ammonia hardening of porous silica antireflective coatings, International Symposium on Optics, Imaging, and Instrumentation (1994) 25-32.

[49] J. G. Wu, J. Wang, T. Shen, Q. Yang, B. Zhang, Z. Zhou, F. Deng, D. Bin, F. Zhang Zhou, Properties of sol-gel derived scratch-resistant nano-porous silica films by a mixed atmosphere treatment, J. Non-cryst. Solids 275 (2000) 169-174.

[50] X. Li, S.A. Jun, scratch-resistant and hydrophobic broadband antireflective coating by sol-gel method, Thin Solid Films 519 (2011) 6236-6240

[51] W. Stöber, A. Fink, Bohn, E. Controlled growth of monodisperse silica spheres in the micron size range, J. Colloid Interf. Sci. 26 (1968) 62-69.

[52] F. Gu, S.F. Wang, M.K. Lv, G.J. Zhou, D. Xu, D.R. Yuan, Photoluminescence Properties of SnO_2 Nanoparticles Synthesized by Sol−Gel Method, J. Phys. Chem. B 108 (2004) 8119-8123

[53] W.P. Jakubik, Surface acoustic wave-based gas sensors, Thin Solid Films, 520 (2011) 986-93.

[54] A.J. Ricco, S.T. Martin, T.E. Zipperian, Surface acoustic wave gas sensor based on film conductivity changes, Sensor. Actuat, 8 (1985) 319333.

[55] V.B. Raj, H. Singh, A.T. Nimal, M.U. Sharma, M. Tomar, V. Gupta, Distinct detection of liquor ammonia by ZnO/SAW sensor: Study of complete sensing mechanism, Sensors and Actuators B: Chemical, 238(2017) 83-90.

Table 1. Measured thickness and sheet conductivity of SiO_2, SnO_2 and SiO_2-SnO_2 films.

Film	Thickness (nm)	σ_{sa}(S/square)	σ_{sg}(S/square)	V_0C_s/σ_{sa}	V_0C_s/σ_{sg}
SiO_2	142	2.8×10^{-11}	7×10^{-11}	5639	2255
SnO_2	128	0.7×10^{-9}	2.45×10^{-9}	226	65
SiO_2-SnO_2	131	0.65×10^{-9}	1.02×10^{-9}	243	155

Note: σ_{sa} = Sheet conductivity of the film in ambient air; σ_{sg} = Sheet conductivity of the film in 10 ppm NH_3.

Table 2. Variation of frequency of the SAW devices when RH is varied.

Relative Humidity Variation	Frequency Shift (KHz)		
	SiO_2	SnO_2	SiO_2-SnO_2
From 5% to 40%	-143	-15.4	-86.4
From 40% to 70%	-105.6	-10.3	-57.2

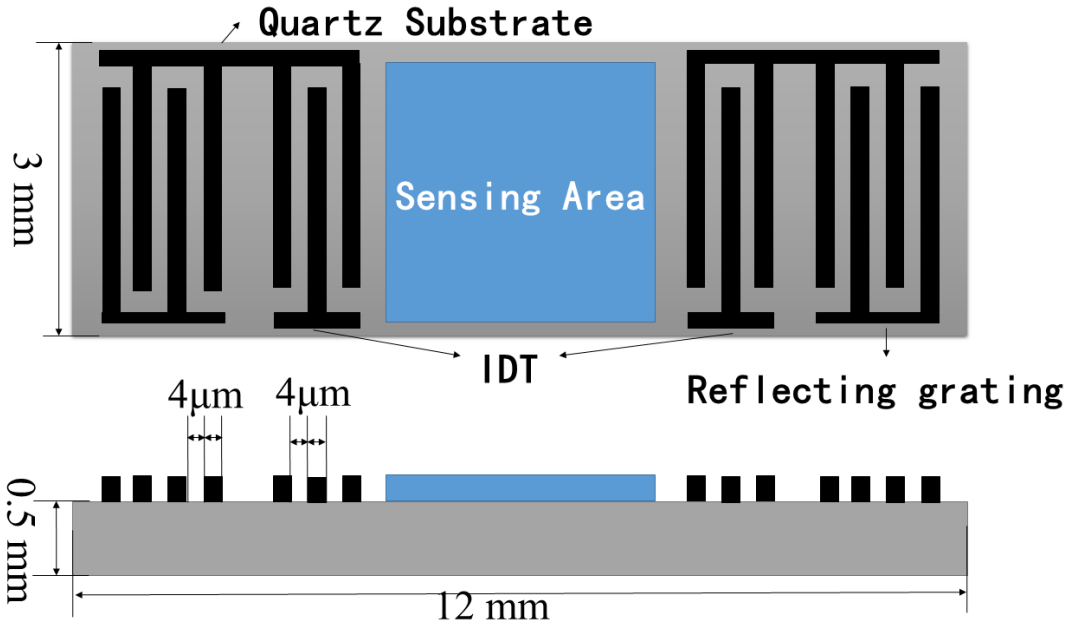

Fig.1. Structure of SAW device.

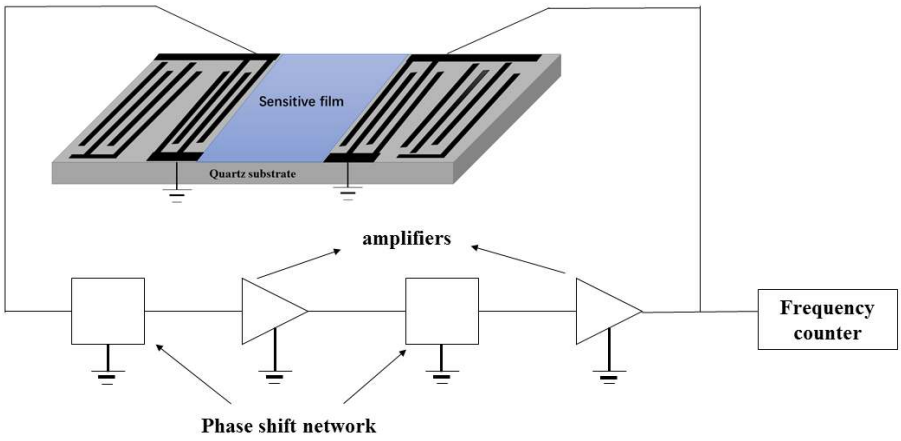

(a)

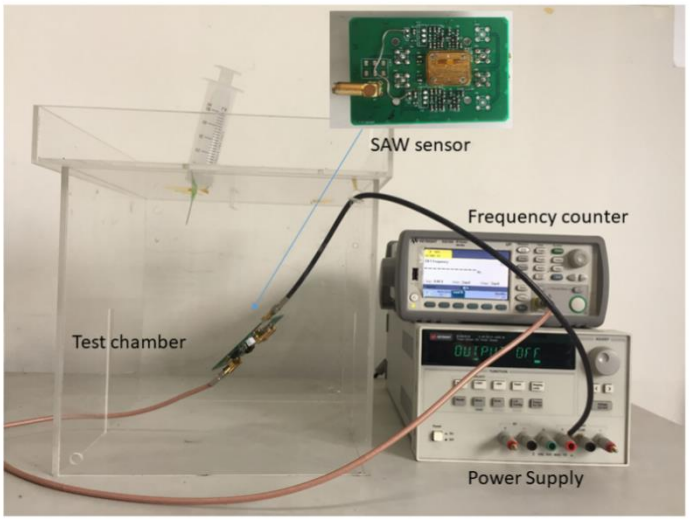

(b)

Figure 2. (a) The structure diagram of a SAW sensor, and (b) SAW gas sensing system.

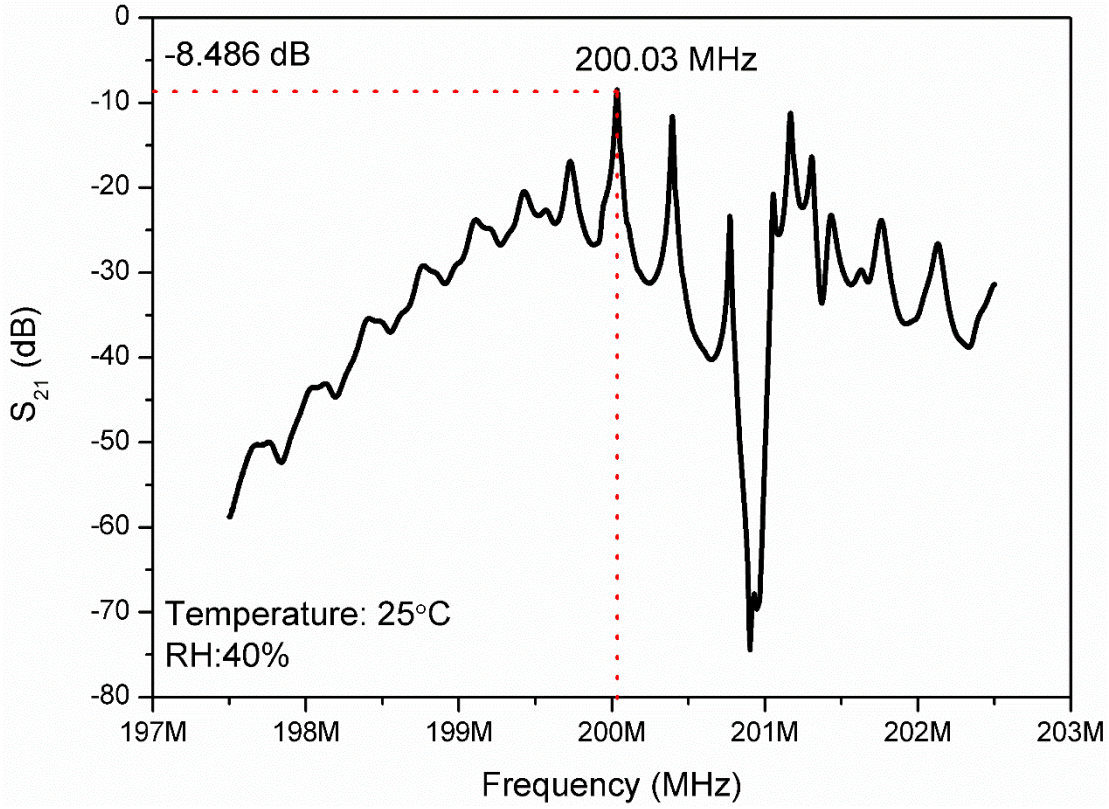

Fig.3. S_{21} parameter of the fabricated SAW device.

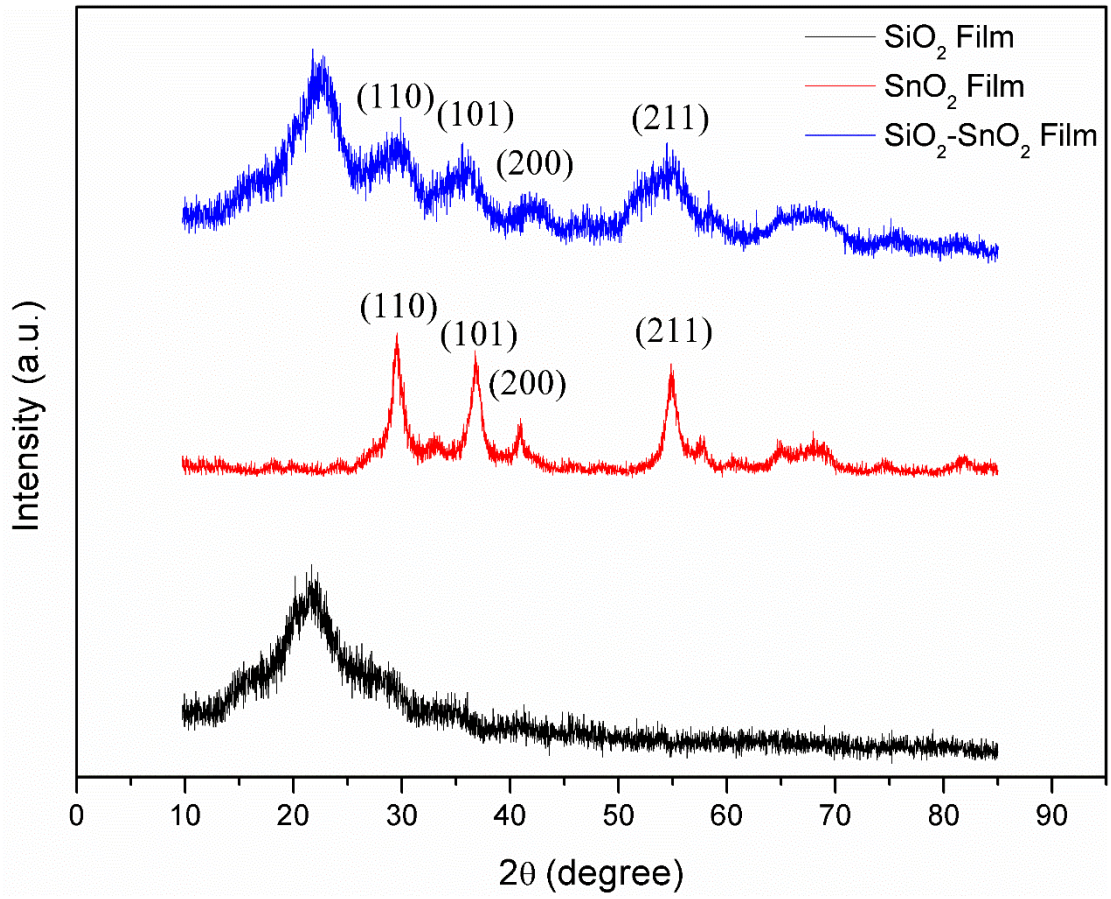

Fig.4. XRD patterns of pristine SiO_2, SnO_2 and SiO_2-SnO_2 composite films.

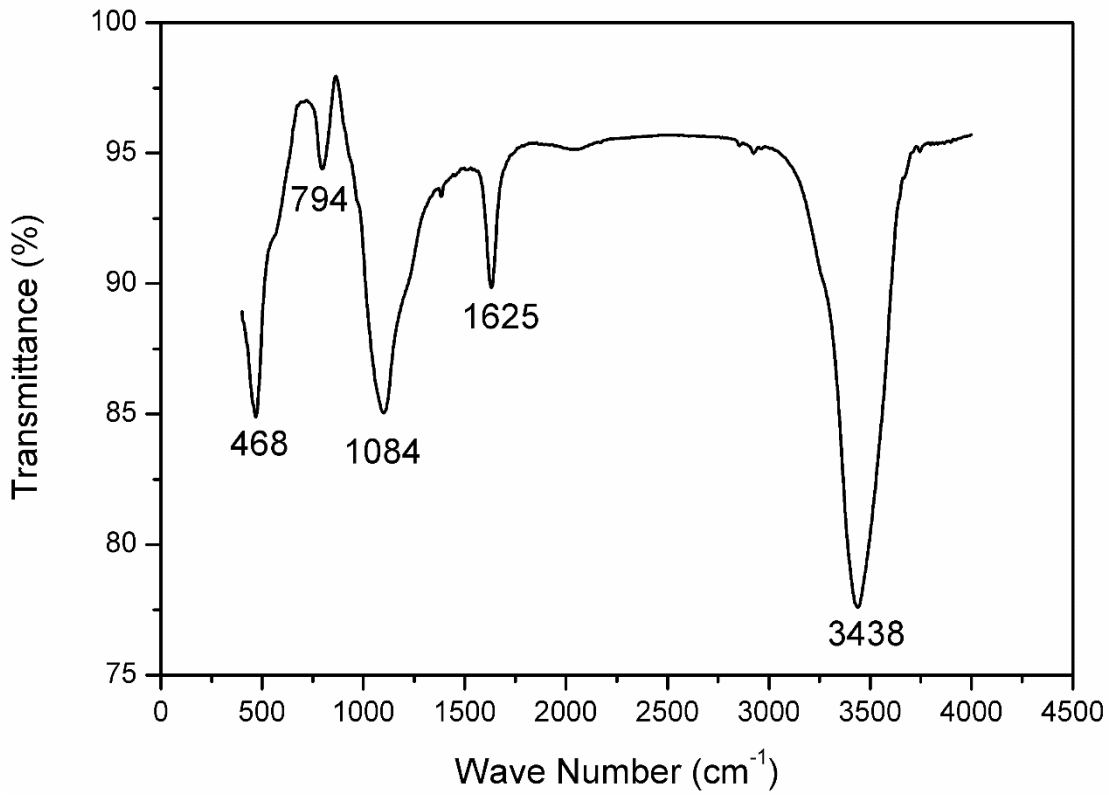
100
95
90
85
80
75
Transmittance (%)
794
1625
468
1084
3438
0
500
1000
1500
2000
2500
3000
3500
4000
4500
Wave Number (cm-1)

(a)

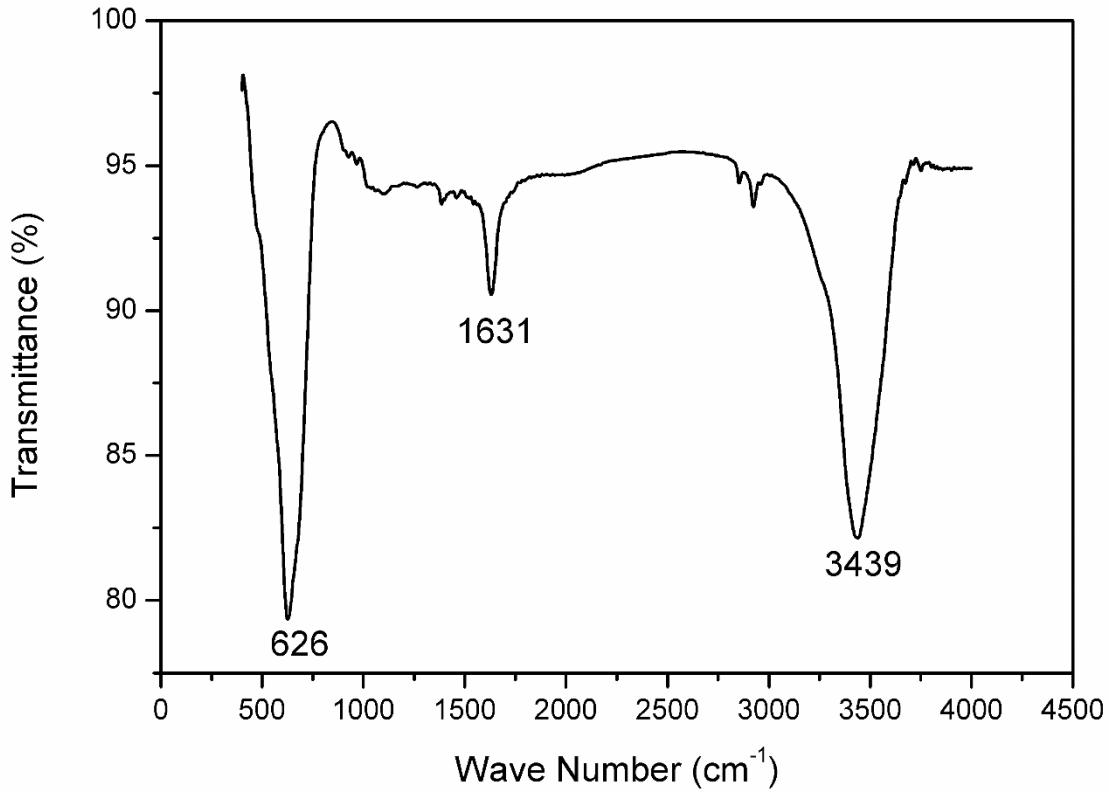
100
95
90
85
80
Transmittance (%)
1631
3439
626
0
500
1000
1500
2000
2500
3000
3500
4000
4500
Wave Number (cm-1)

(b)

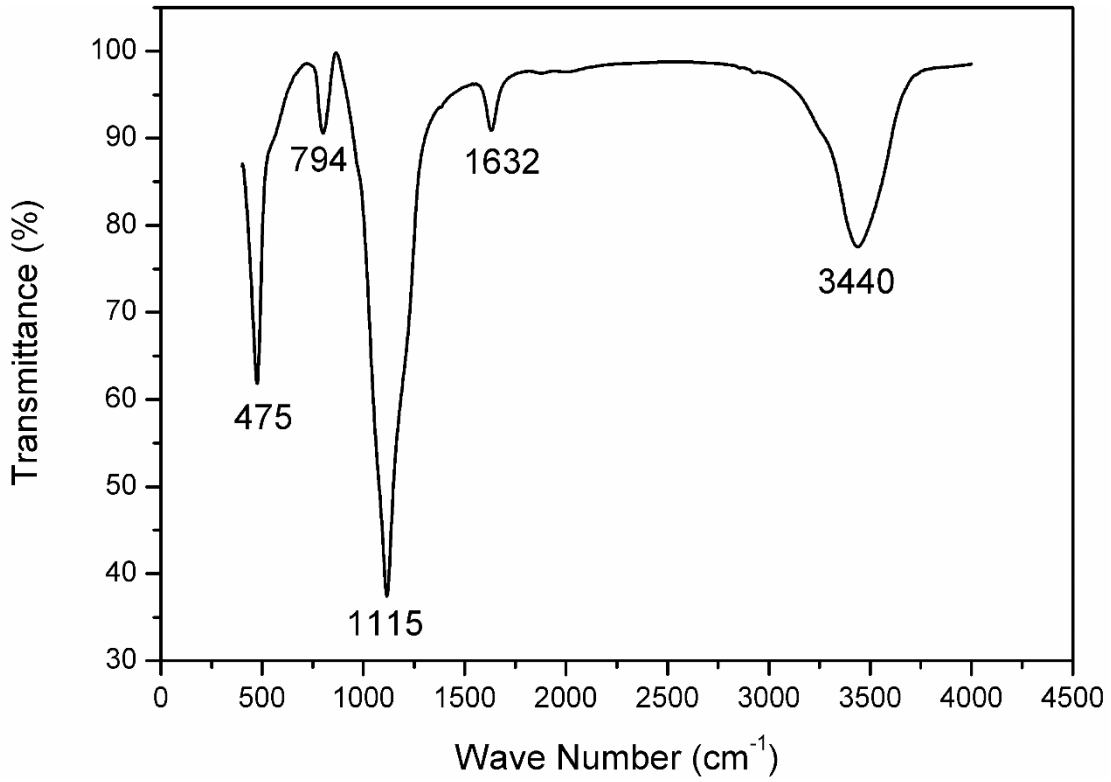

(c)

Fig.5. FTIR spectra of SiO_2 (a), SnO_2 (b) and SiO_2-SnO_2 composite films (c).

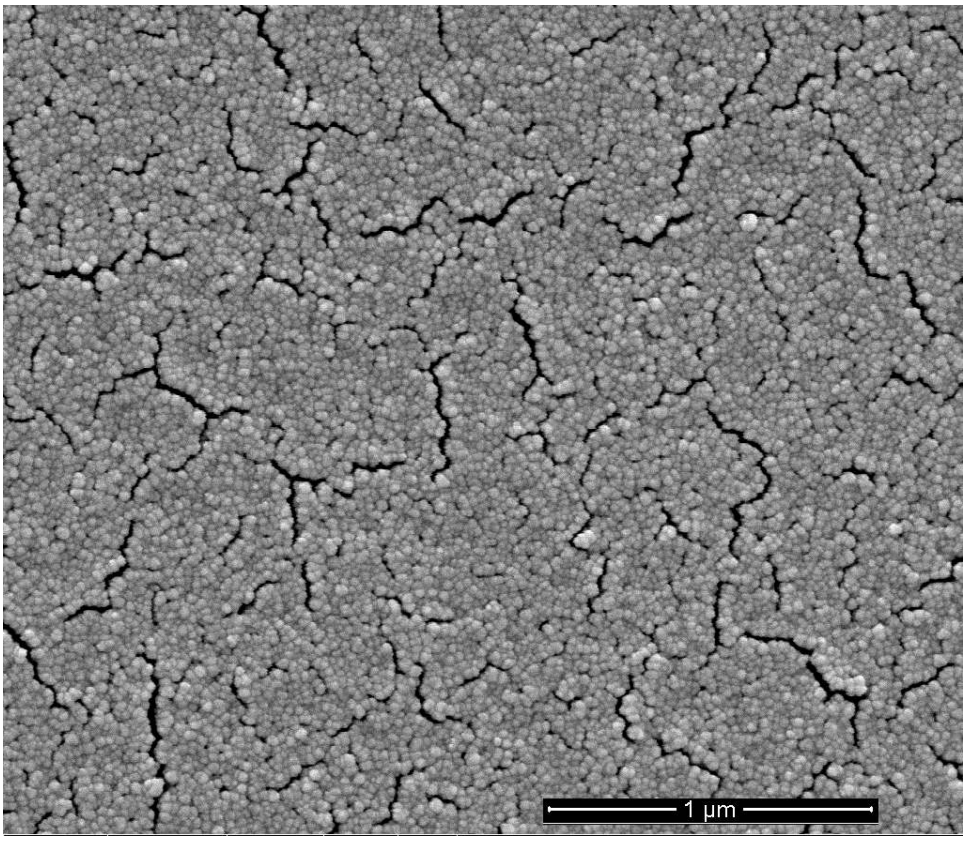

（a）

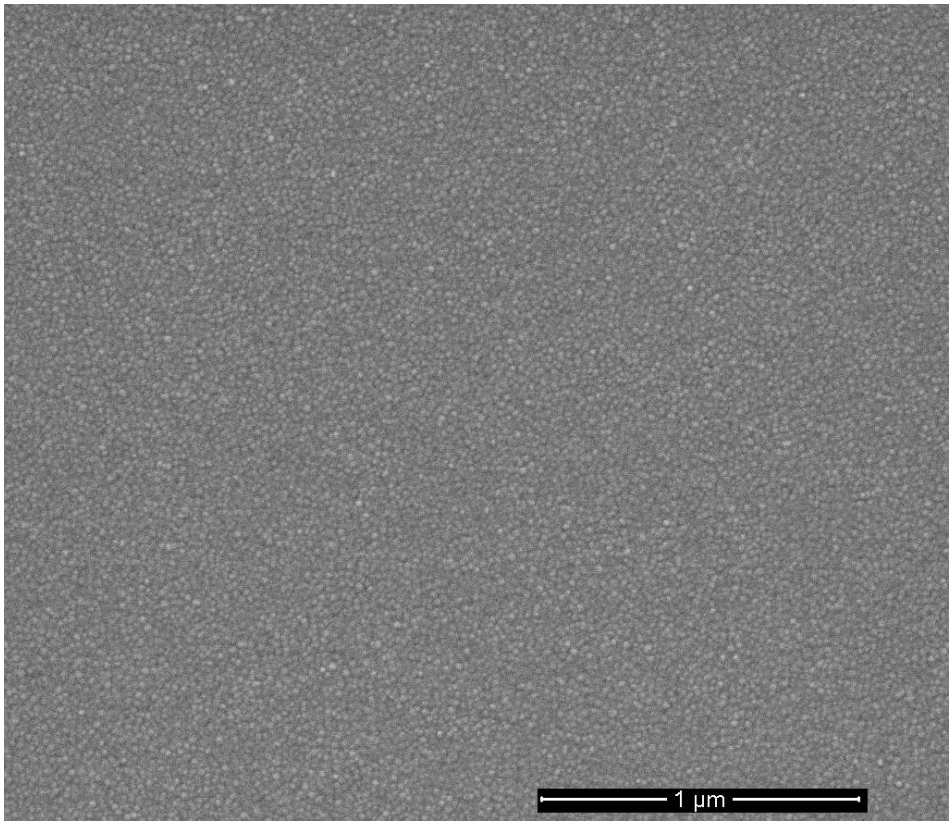

（b）

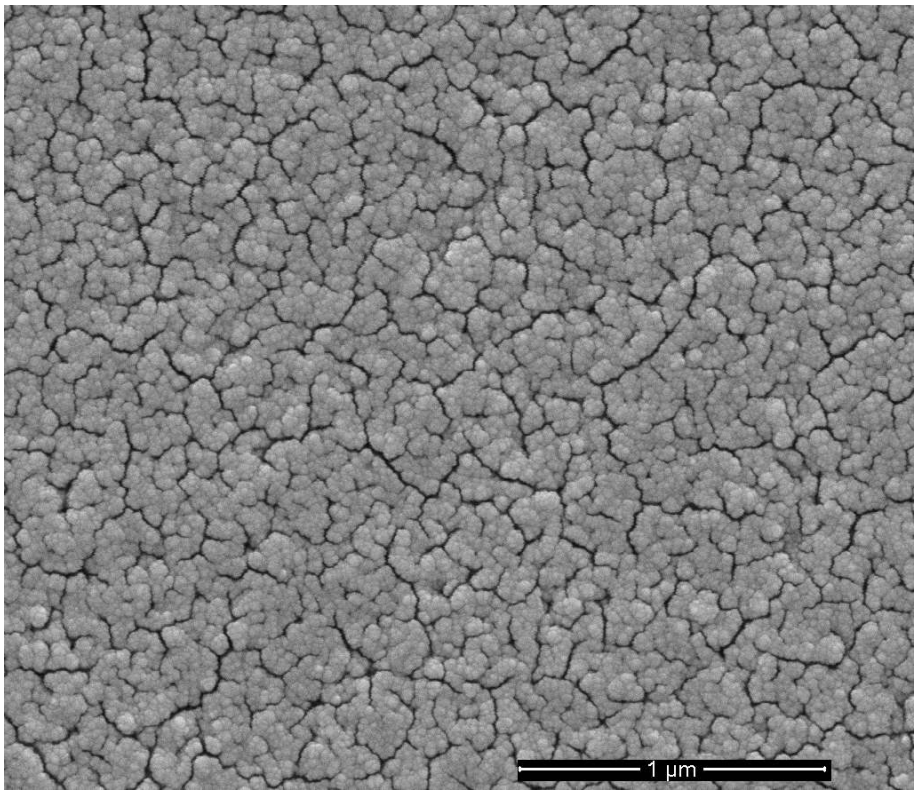

（c）

Fig.6. SEM images of (a) SiO_2, (b) SnO_2 and (c) SiO_2-SnO_2 films.

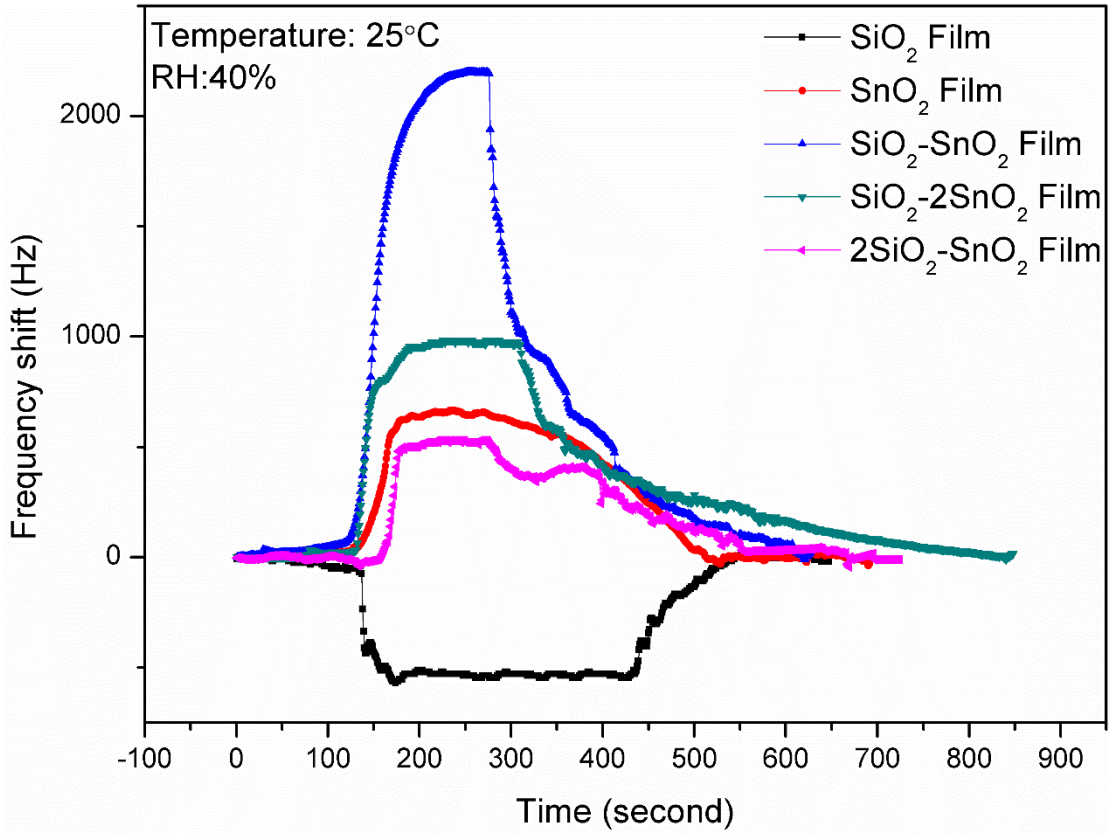

Fig.7. Frequency responses of SAW sensor based on SiO_2, SnO_2, SiO_2-SnO_2, SiO_2-$2SnO_2$ and $2SiO_2$-SnO_2 films to 10 ppm NH_3.

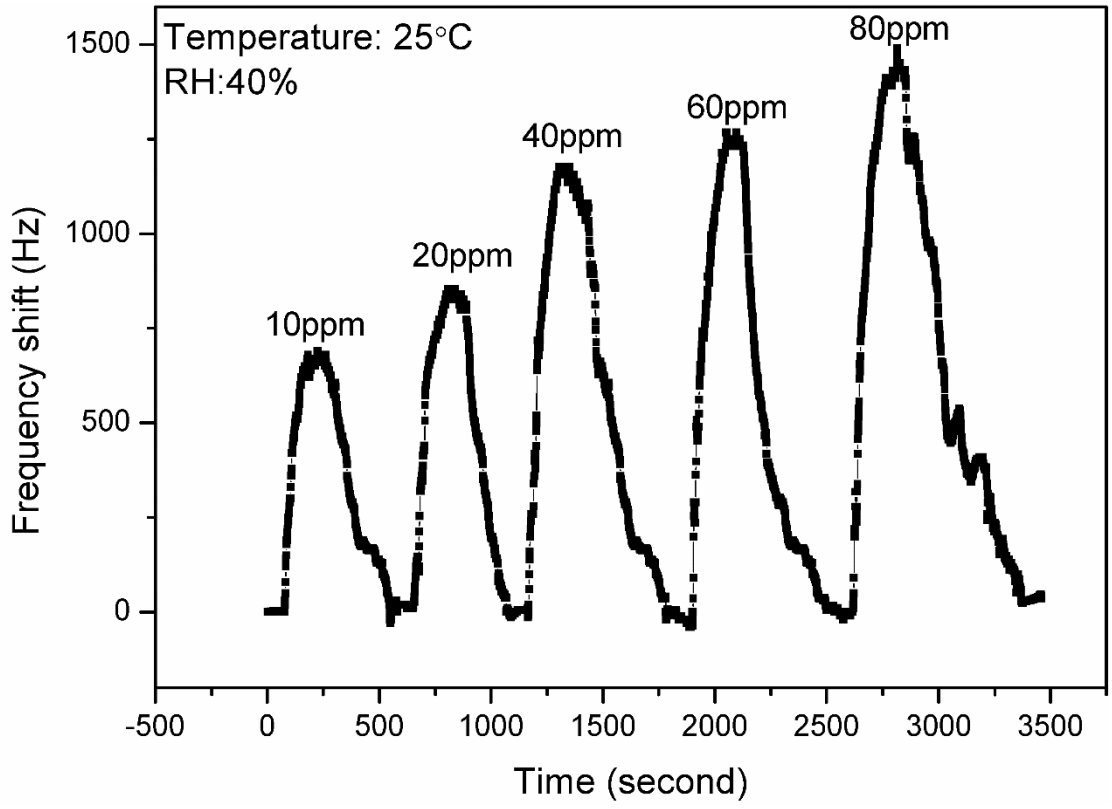

（a）

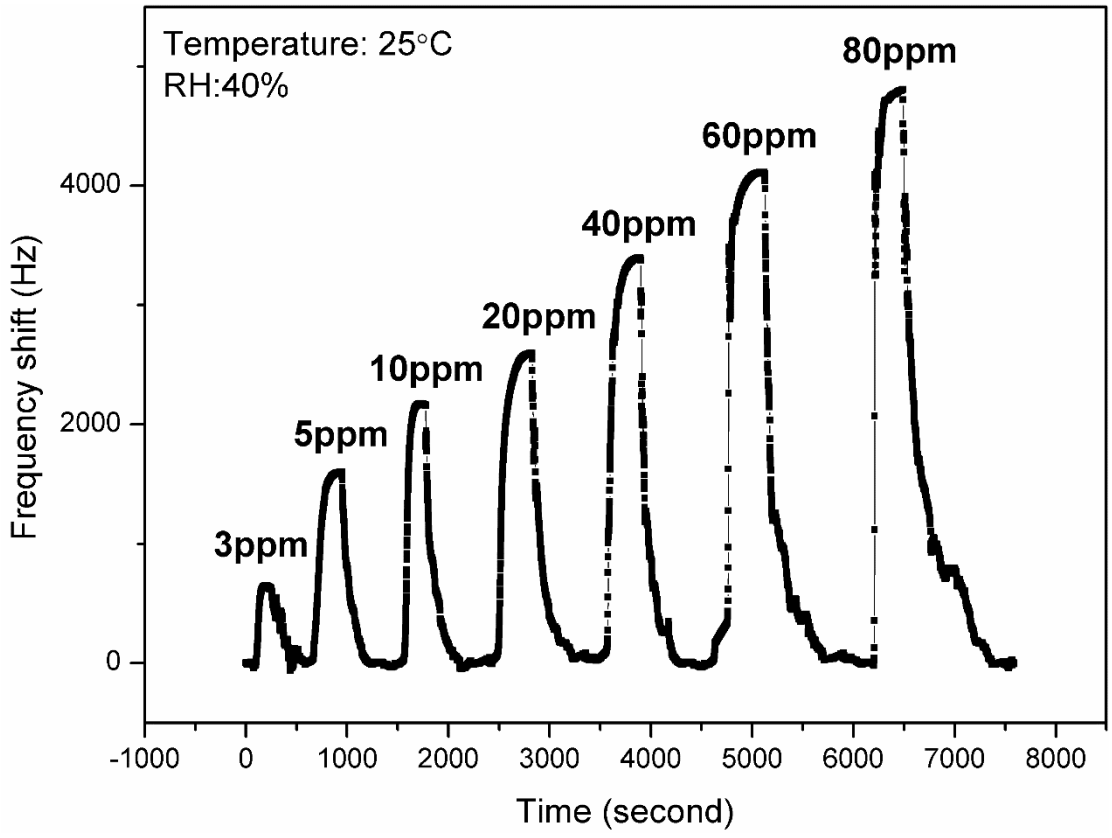

（b）

Fig.8. Dynamic frequency responses to various NH_3 concentrations for the sensor based on （a）pure SnO_2 film（b）SiO_2-SnO_2 film.

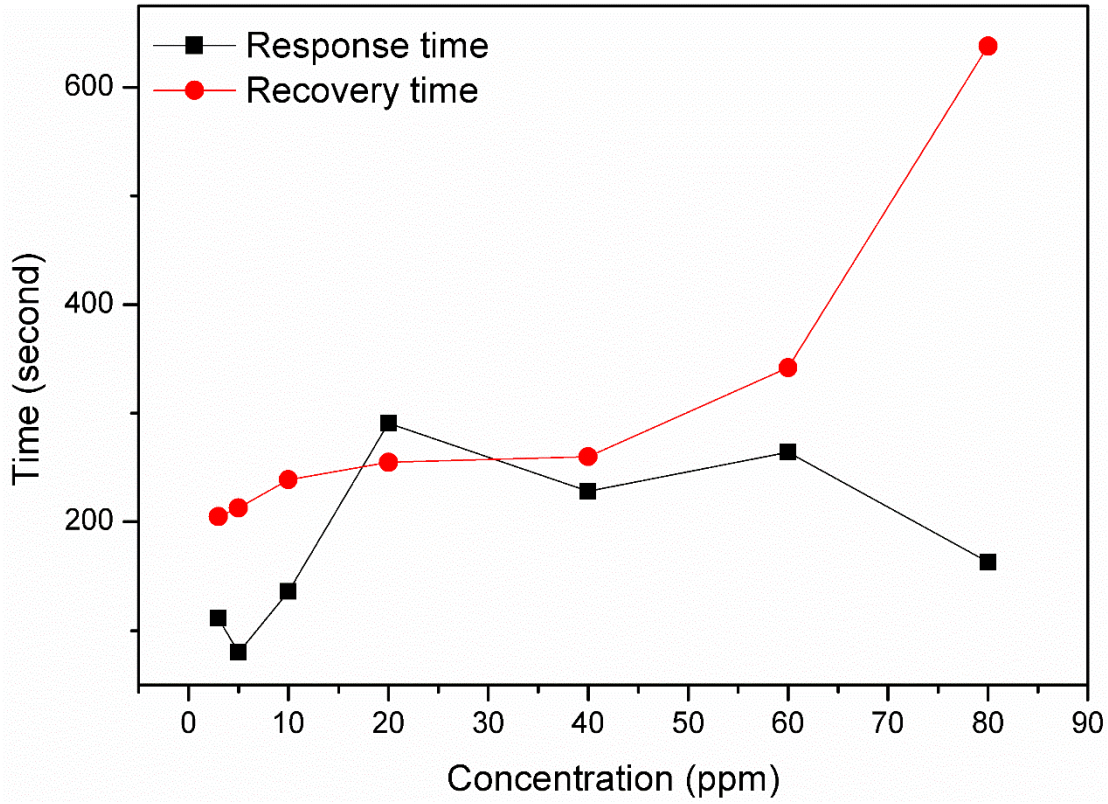

Fig.9. Response and recovery times of SiO_2-SnO_2 as a function of NH_3 concentration.

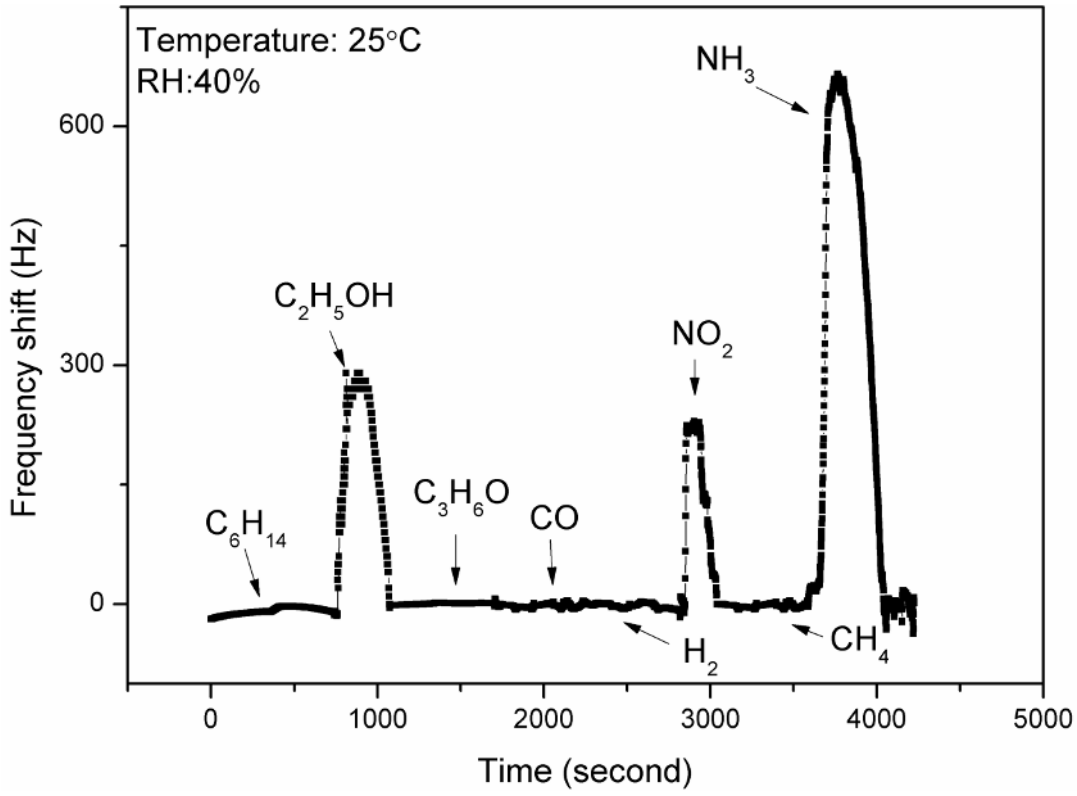

（a）

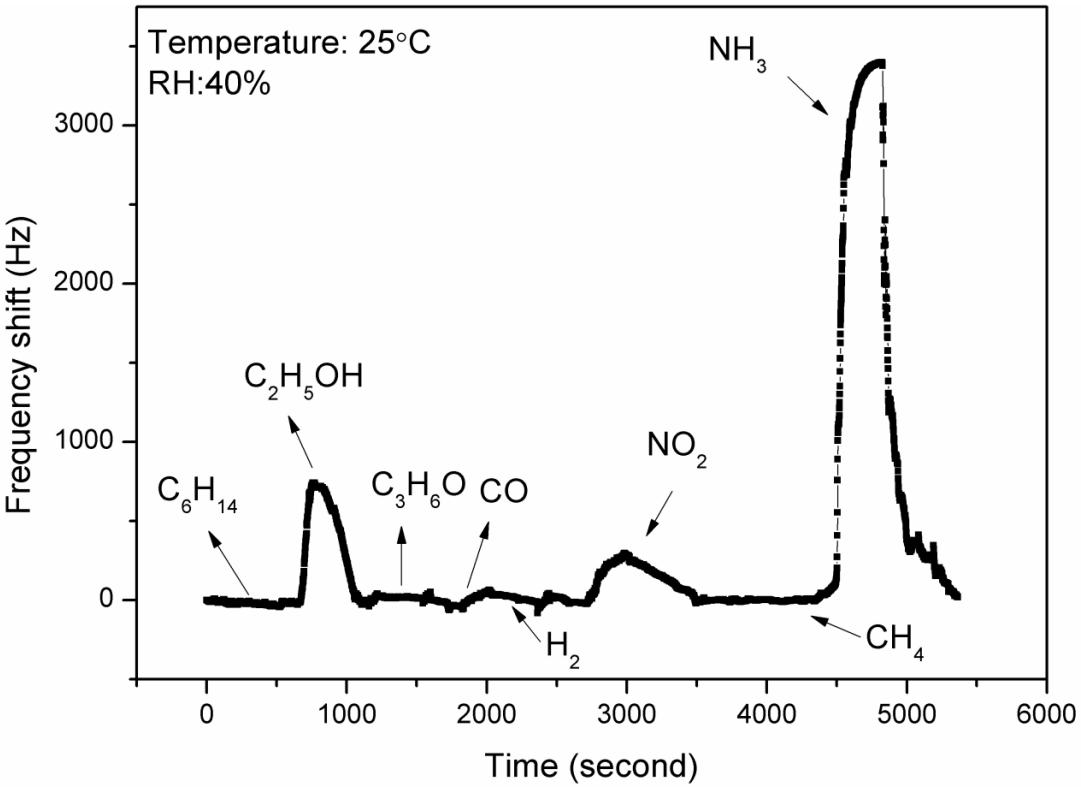

（b）

Fig.10. Dynamic response and recovery of the sensor based on (a) pure SnO_2 film to various gases (10 ppm C_6H_{14}, C_2H_5OH, C_3H_6O, CO, H_2, NO_2 and CH_4 and NH_3). (b) SiO_2-SnO_2 film to various gases (50 ppm C_6H_{14}, C_2H_5OH, C_3H_6O, CO, H_2, NO_2, CH_4 and 20 ppm

NH_3).

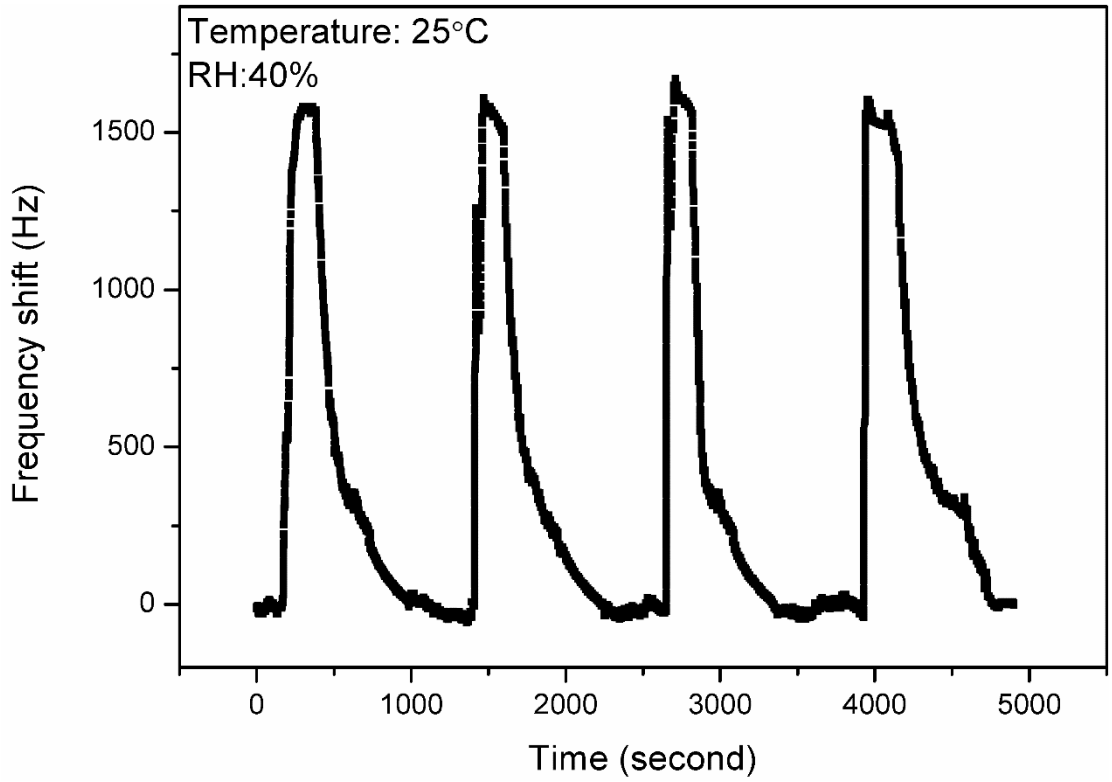

Fig.11. Repeatability tests of dynamic response and recovery of the sensor based on SiO_2-SnO_2 film to 5 ppm NH_3 for 4 cycles.

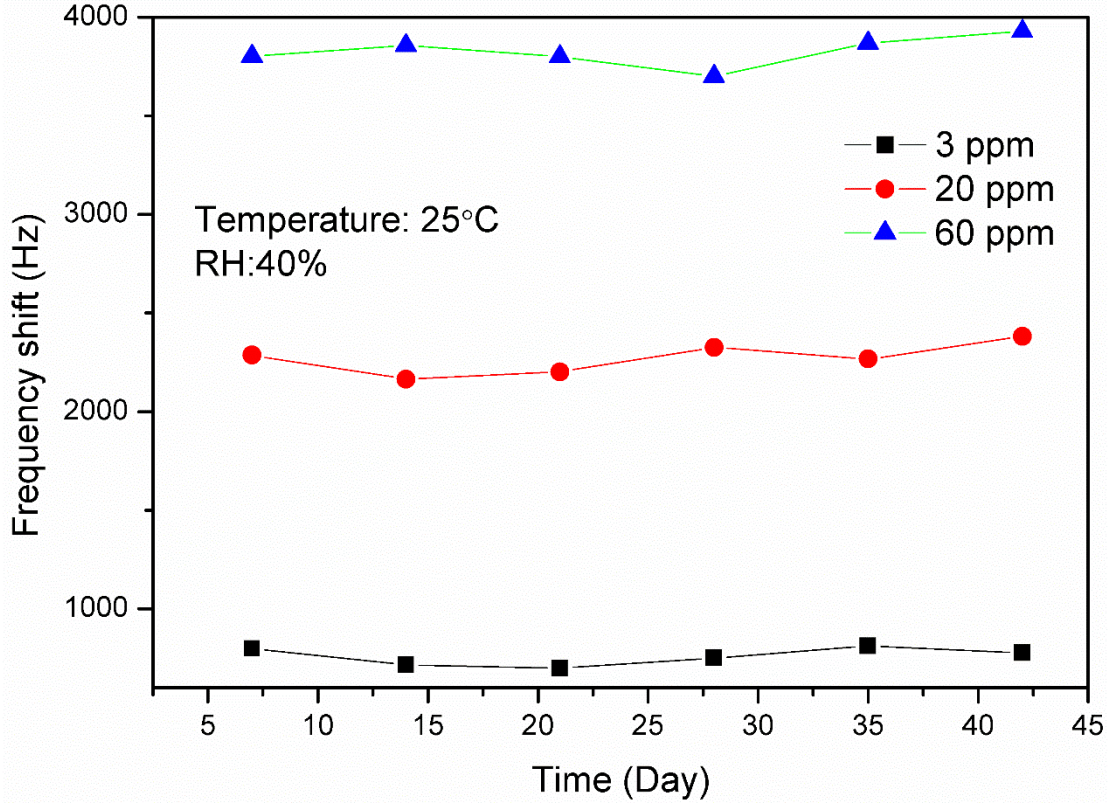

Fig.12. Frequency shift of the sensor based on SiO_2-SnO_2 film to NH_3 of various concentrations in 42 days.

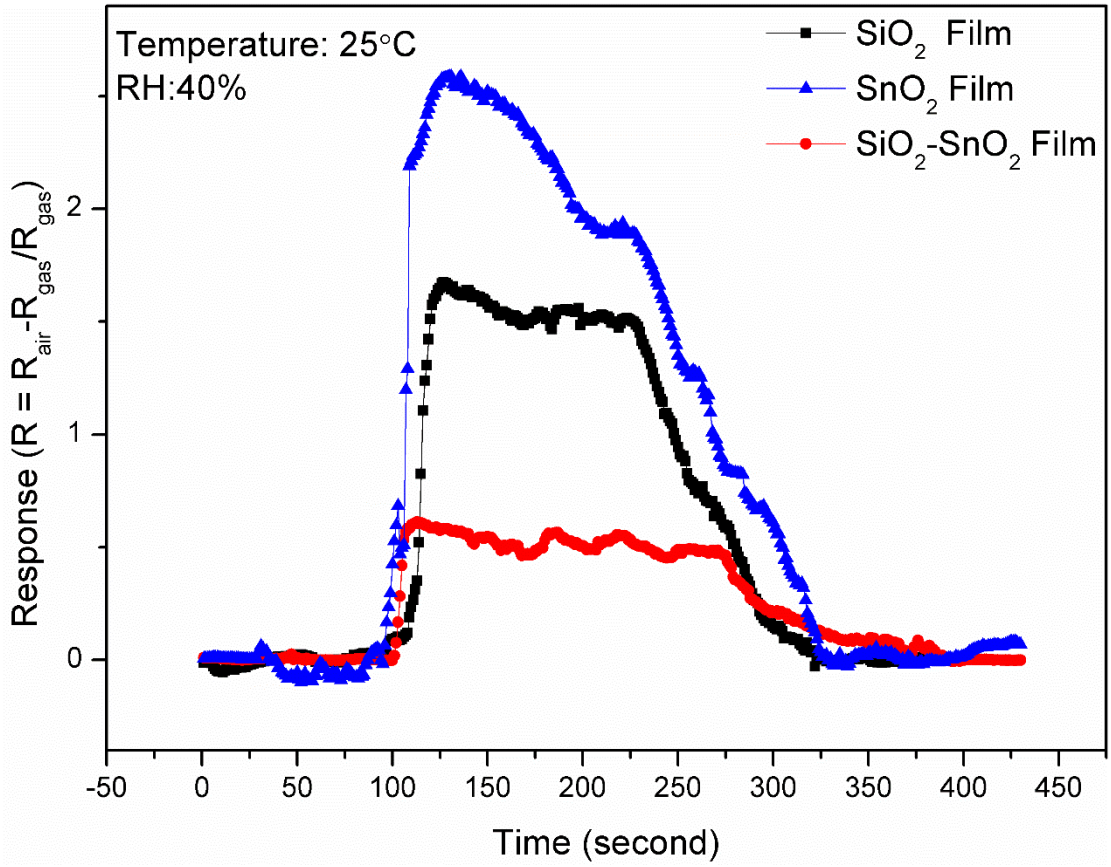

Fig.13. Electrical response of the SiO_2, SnO_2 and SiO_2-SnO_2 films to 10 ppm NH_3.

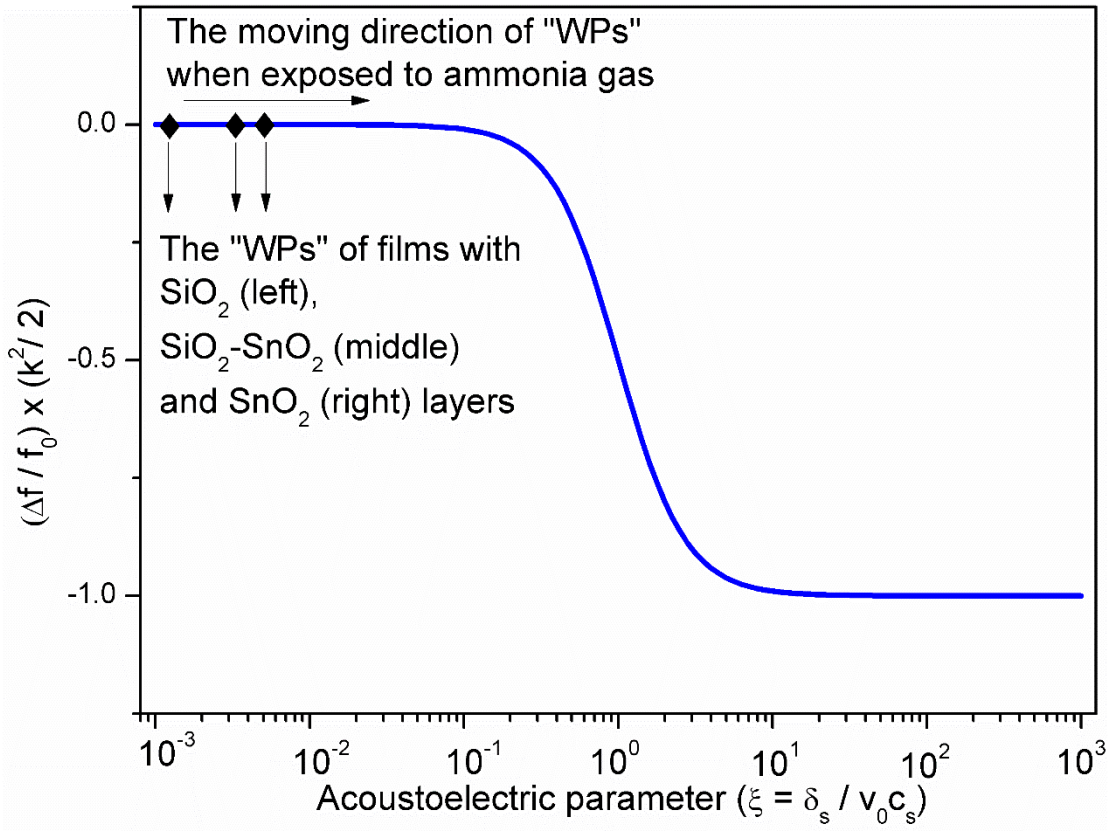

Fig. 14. Plot of velocity changes versus acoustoelectric parameter ξ . (The "WP" in brackets indicates working point.)

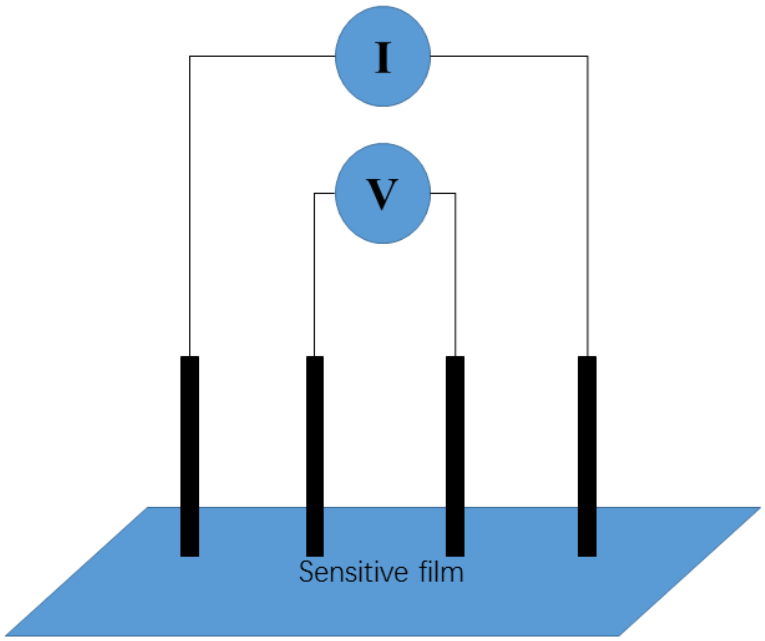

Fig. 15. Four probe test conductivity schematic.

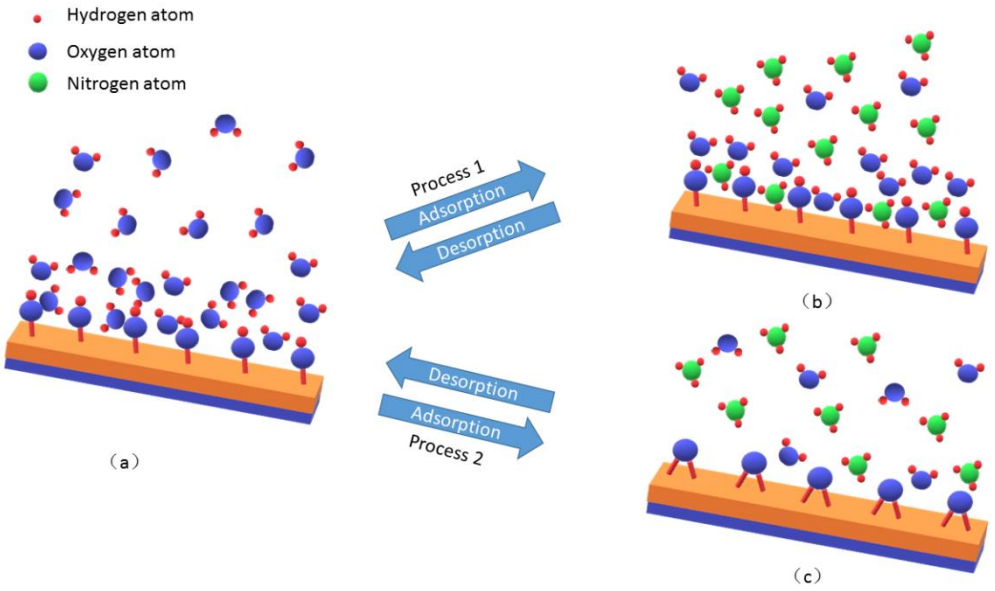

Fig. 16. Sensing principle of a film with hydroxyl groups. (a) The sensing film in ambient air, H_2O is absorbed on the film. (b)Process 1: NH_3 is absorbed by the H_2O on the film. (c) Process 2: NH_3-catalyzed film condensation leads to condensation reaction.

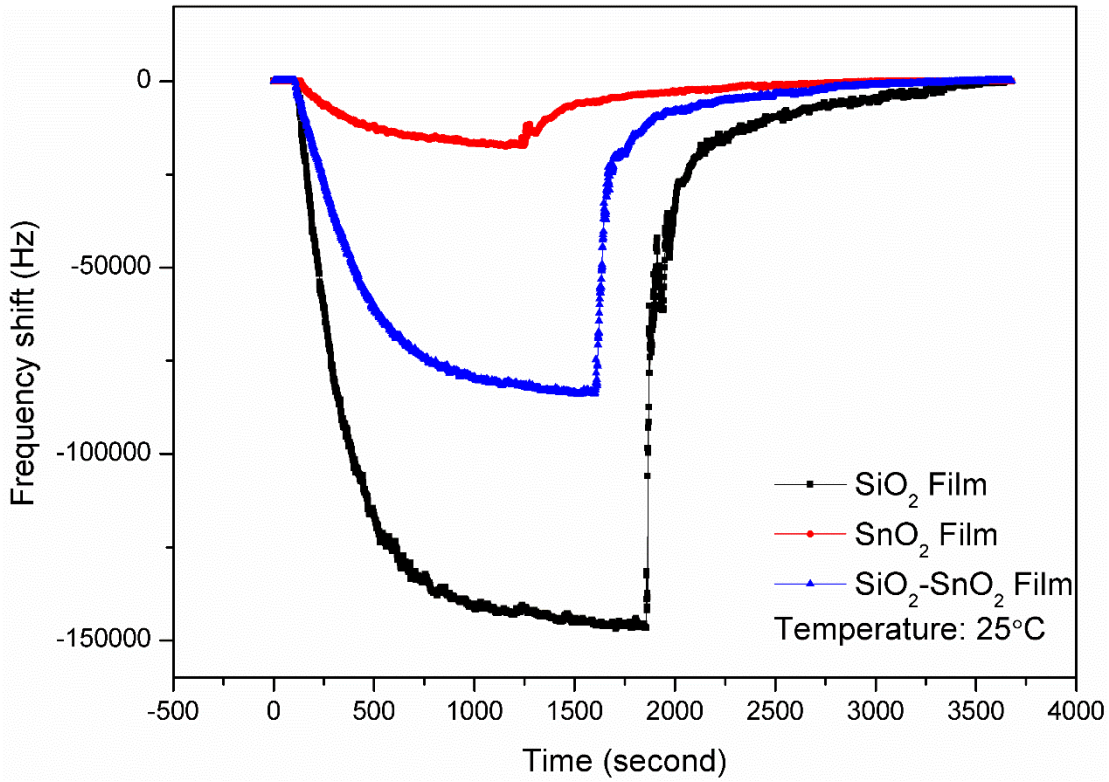

（a）

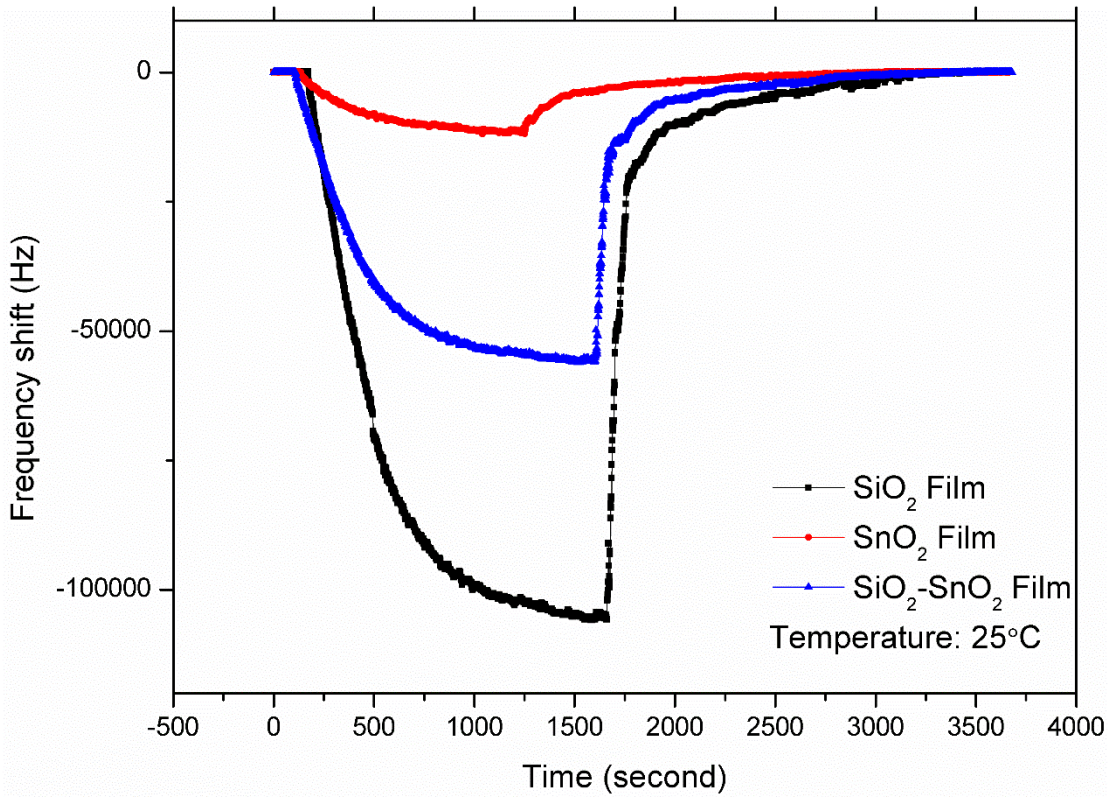

（b）

Fig. 17. Frequency shift when relative humidity changes (a) from 5% to 40% (b) from 40% to 70%.

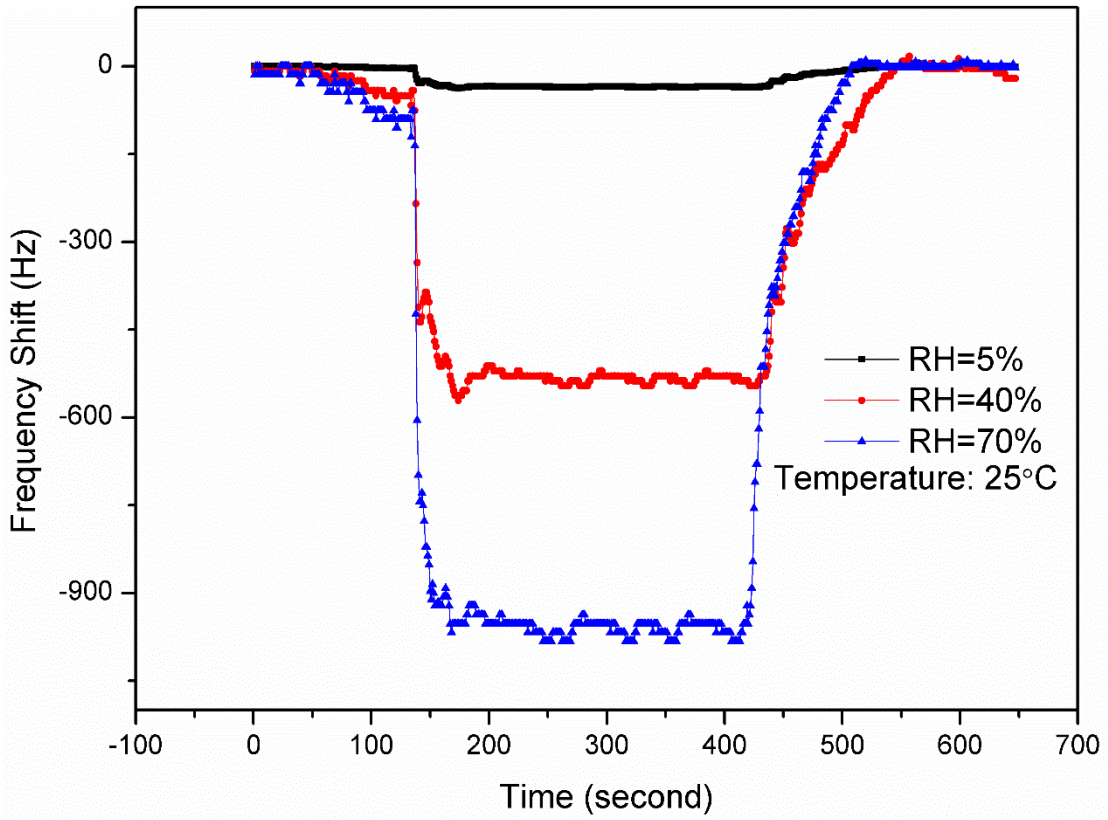
0
-300
-600
-900
Frequency Shift (Hz)
-100
0
100
200
300
400
500
600
700
Time (second)
RH=5%
RH=40%
RH=70%
Temperature: 25°C

（a）

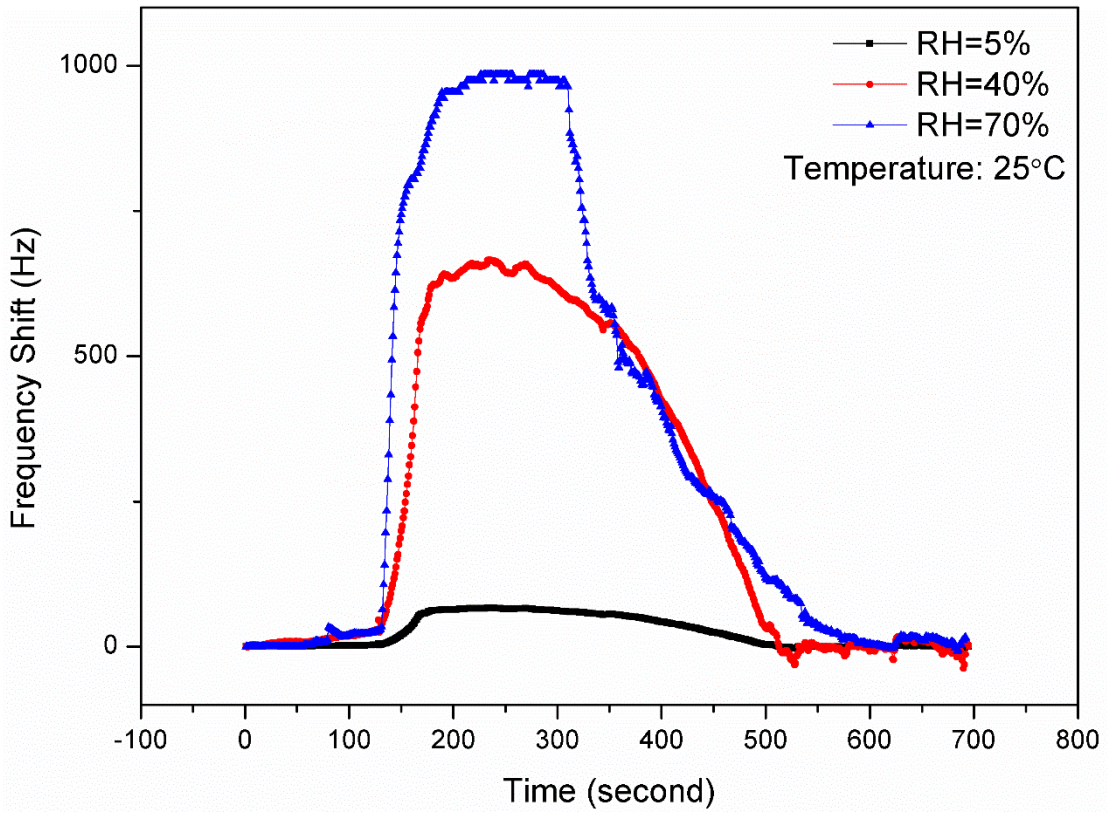
1000
500
0
Frequency Shift (Hz)
-100
0
100
200
300
400
500
600
700
800
Time (second)
RH=5%
RH=40%
RH=70%
Temperature: 25°C

（b）

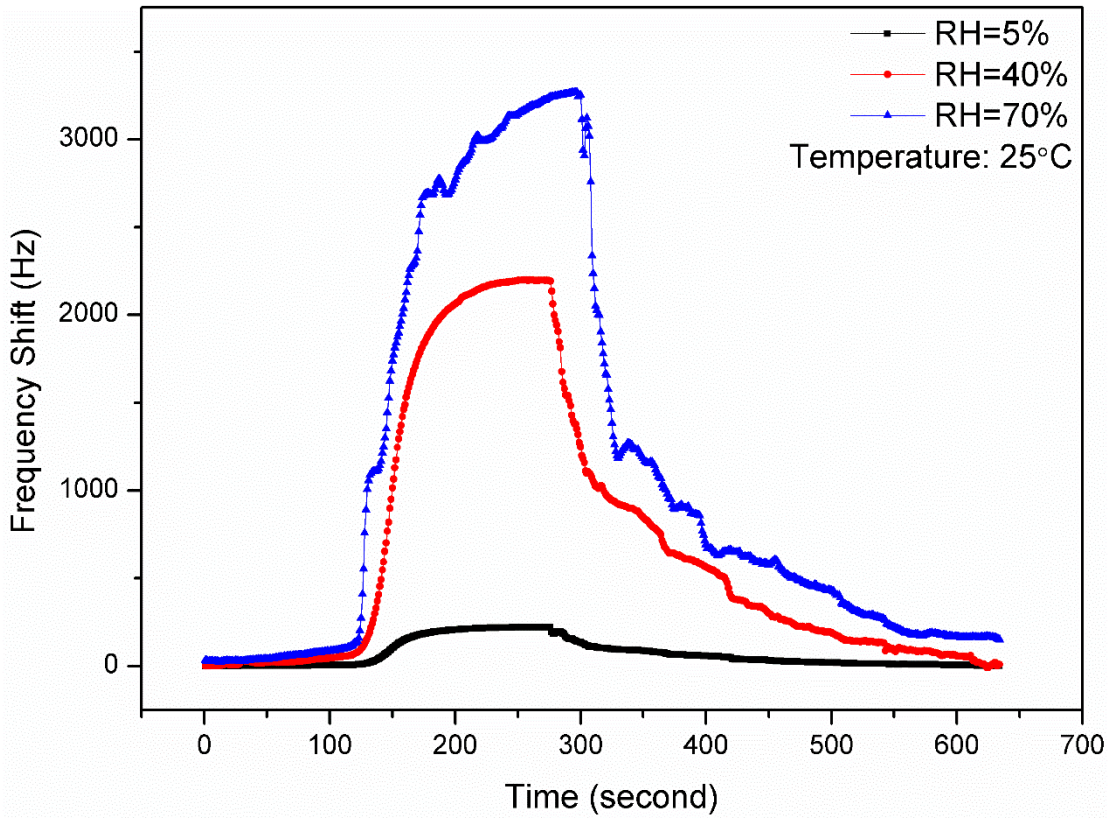

（c）

Fig. 18. Response of SAW sensors based on SiO_2 (a), SnO_2 (b) and SiO_2-SnO_2 (c) films to 10 ppm NH_3 at room temperature of 25° C with different relative humidity.

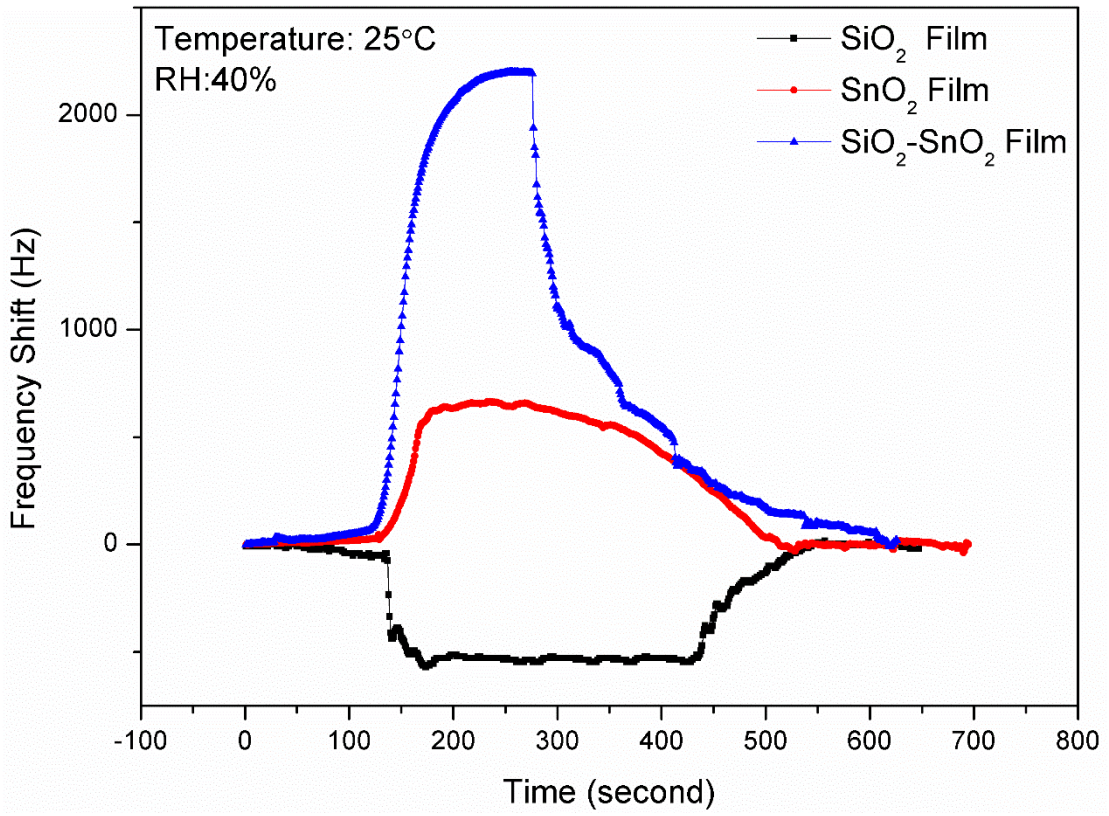

Fig. 19. Comparison of frequency response and recovery process to 10 ppm NH_3 with RH = 40% between the SAW sensors based on SiO_2, SnO_2 and SiO_2-SnO_2 films.